Probing QCD dynamics and the standard model with $D_{(s)} \to P^+P^0\gamma$ decays

Nico Adolph[1,*] and Gudrun Hiller[1,†]

[1] *Fakultät Physik, TU Dortmund, Otto-Hahn-Str.4, D-44221 Dortmund, Germany*

We compute 10 radiative three-body decays of charged charmed mesons $D^+ \to P^+P^0\gamma$ and $D_s \to P^+P^0\gamma$, $P = \pi, K$, in leading order QCDF, HHχPT and the soft photon approximation. We work out decay distributions and asymmetries in the standard model and with new physics in the electromagnetic dipole operators. The forward-backward asymmetry is suitable to probe the QCD frameworks, in particular the s-channel dependent weak annihilation contributions in QCDF against the markedly different resonance structure in HHχPT. These studies can be performed with Cabibbo-favored modes $D_s \to \pi^+\pi^0\gamma$, $D^+ \to \pi^+\overline{K}^0\gamma$ and $D_s \to K^+\overline{K}^0\gamma$ with $\mathcal{O}(10^{-4} - 10^{-3})$-level branching ratio, which are standard model-like and induced by different hadronic dynamics. Understanding of the latter can therefore be improved in a data-driven way and sharpens the interpretation of standard model tests. Singly Cabibbo-suppressed modes such as $D^+ \to \pi^+\pi^0\gamma$, $D_s \to \pi^+K^0\gamma$, $D_s \to K^+\pi^0\gamma$ with branching ratios within $\sim 10^{-5} - 10^{-4}$ are sensitive to new physics that can be signalled in the forward-backward asymmetry and in the CP-asymmetry of the rate, ideally in the Dalitz region but also in single differential distributions. Results complement those with neutral $D^0 \to PP\gamma$ decays.

arXiv:2104.08287v1 [hep-ph] 16 Apr 2021

I. INTRODUCTION

Rare semileptonic and radiative charm decays are sensitive to the flavor sector in and beyond the standard model [1]. They are accessible to precision study at the LHC [2], the Belle II [3], and BES III experiments [4], and complement searches in beauty and kaon decays. Disentangling resonance contributions from those of BSM physics is key, and particularly challenging in charm as the charm quark mass is not as well separated from the QCD scale as the b-quark mass, and branching ratios are often dominated by resonances on and off peak. A well-known workaround strategy is to use null tests, that is, observables designed to have an unmeasurably small or otherwise controlled SM background, due to protection by approximate symmetries of the SM [5–7]. On the other hand, the D-system is advantageous as many partner modes exist which are linked by swapping light quarks,

*Electronic address: nico.adolph@tu-dortmund.de
†Electronic address: gudrun.hiller@tu-dortmund.de

or flavor symmetry. A combined analysis of these partner modes allows therefore to gain insights into the resonance dynamics and new physics simultaneously, as shown for instance for radiative decays in [8, 9].

In this regard, radiative three-body D-decays turn out to be a useful laboratory to explore QCD dynamics and to test the SM. Here we consider, in total ten, Cabibbo-favored (CF), singly Cabibbo-suppressed (SCS), and doubly Cabibbo-suppressed (DCS) decays of D^+ and D_s mesons

$$\begin{aligned}
&\text{CF:} \quad D_s \to \pi^+\pi^0\gamma\,,\ D_s \to K^+\overline{K}^0\gamma\,,\ D^+ \to \pi^+\overline{K}^0\gamma\,,\ (D^0 \to \pi^0\overline{K}^0\gamma\,,\ D^0 \to \pi^+K^-\gamma)\\
&\text{SCS:} \quad D^+ \to \pi^+\pi^0\gamma\,,\ D_s \to \pi^+K^0\gamma\,,\ D_s \to K^+\pi^0\gamma\,,\\
&\qquad\ D^+ \to K^+\overline{K}^0\gamma\,, (D^0 \to \pi^+\pi^-\gamma\,,\ D^0 \to K^+K^-\gamma)\\
&\text{DCS:} \quad D^+ \to \pi^+K^0\gamma\,, D^+ \to K^+\pi^0\gamma\,,\ D_s \to K^+K^0\gamma
\end{aligned} \tag{1}$$

The D^0 decays given in parentheses are covered in [10]. The modes $D^+ \to K^+K^0\gamma$ and $D_s \to \pi^+\overline{K}^0\gamma$ are $|\Delta s| = 2$ processes and are not induced by dimension 6 operators, and not considered in this works. Three-body radiative D decays have been investigated previously in [11, 12].

As in [10] we work out decay amplitudes in different QCD frameworks: leading order QCD factorization (QCDF), heavy hadron chiral perturbation theory (HHχPT) and the soft photon approximation, each of which is expected to hold in specific regions of phase space. We show that the forward-backward asymmetry efficiently disentangles different resonance contributions and therefore probes the QCD frameworks. These tests can be performed with SM-like modes, the CF and DCS ones from (1), and assist NP searches in the SCS ones.

This paper is organized as follows: In Sec. II we give the kinematics and observables for $D \to PP\gamma$ decays, the weak effective low energy Lagrangian and briefly review QCD frameworks. We also present the weak annihilation contribution in QCDF. Analytical results in HHχPT are presented in Appendix A. SM predictions are shown in Sec. III. We work out predictions with BSM physics in Sec. IV. In Sec. V we summarize. In appendix A we provide HHχPT-amplitudes and Feynman diagrams for CF, SCS and DCS modes, and a list of differences we found with previous works [11] on $D^+ \to \pi^+\overline{K}^0\gamma$ in appendix B.

II. GENERALITIES

A. Kinematics and observables

The double differential decay rate of the radiative three-body decay $D^+_{(s)}(P) \to P^+(p_1)P^0(p_2)\gamma(k,\epsilon^*)$ can be written as [10]

$$\begin{aligned}\frac{d^2\Gamma}{dsdt} &= \frac{|A_-|^2+|A_+|^2}{128(2\pi)^3 m_D^3} \\ &\times \left[m_1^2(t-m_2^2)(s-m_D^2) - m_2^4 m_D^2 - st(s+t-m_D^2) + m_2^2(st+(s+t)m_D^2 - m_D^4)\right],\end{aligned} \tag{2}$$

where the parity-even ($\mathcal{A}_+$) and parity-odd ($\mathcal{A}_-$) contributions are defined by the general Lorentz decomposition of the decay amplitude

$$\mathcal{A}(D^+_{(s)} \to P^+P^0\gamma) = A_-(s,t)\left[(p_1\cdot k)(p_2\cdot\epsilon^*) - (p_2\cdot k)(p_1\cdot\epsilon^*)\right] + A_+(s,t)\epsilon^{\mu\alpha\beta\gamma}\epsilon^*_\mu p_{1\alpha}p_{2\beta}k_\gamma\,. \tag{3}$$

The subscript 1 (2) of four-momenta and masses refer to the (un)charged final state P^+ (P^0), while the initial state $D^+_{(s)}$-meson is denoted by capital letters. Furthermore, $s=(p_1+p_2)^2$, $t=(p_2+k)^2$ and $u=(p_1+k)^2 = m_D^2+m_1^2+m_2^2-s-t$. We employ m_D for both the D^+ and the D_s mass and specify the spectator quark only when needed. The polarization vector of the photon is denoted by ϵ.

The three-body decay allows to define a forward-backward asymmetry [10]

$$\begin{aligned}A_{\rm FB}(s) &= \frac{\int_{t_{\rm min}}^{t_0} dt\frac{d^2\Gamma}{dsdt} - \int_{t_0}^{t_{\rm max}} dt\frac{d^2\Gamma}{dsdt}}{\int_{t_{\rm min}}^{t_0} dt\frac{d^2\Gamma}{dsdt} + \int_{t_0}^{t_{\rm max}} dt\frac{d^2\Gamma}{dsdt}}\,, \\ t_{\rm min} &= \frac{(m_D^2-m_1^2+m_2^2)^2}{4s} - \left(\sqrt{\frac{(s-m_1^2+m_2^2)^2}{4s}-m_2^2} + \frac{m_D^2-s}{2\sqrt{s}}\right)^2, \\ t_{\rm max} &= \frac{(m_D^2-m_1^2+m_2^2)^2}{4s} - \left(\sqrt{\frac{(s-m_1^2+m_2^2)^2}{4s}-m_2^2} - \frac{m_D^2-s}{2\sqrt{s}}\right)^2, \\ t_0 &= \frac{1}{2s}\left(-s^2+s(m_D^2+m_1^2+m_2^2)+m_D^2(m_2^2-m_1^2)\right),\end{aligned} \tag{4}$$

where the first (second) term in the numerator corresponds to $0\le\cos(\theta_{2\gamma})\le 1$ ($-1\le\cos(\theta_{2\gamma})\le 0$). Here, $\theta_{2\gamma}$ is the angle between P^0 and the photon in the P^+-P^0 center-of-mass frame. If the forward-backward asymmetry would be defined in terms of $\cos(\theta_{1\gamma})$, one would obtain an additional minus sign in the definition of $A_{\rm FB}$. The $A_{\rm FB}$ turns out to be suitable to distinguish resonance contributions in s-channel (in PP), versus t,u-channel ones (in $P\gamma$) in the decay amplitudes.

The most promissing observable to test for BSM physics is the single- or double-differential CP asymmetry defined as respectively, by

$$A_{\rm CP}(s) = \int dt A_{\rm CP}(s,t)\,, \quad A_{\rm CP}(s,t) = \frac{1}{\Gamma+\overline{\Gamma}}\left(\frac{d^2\Gamma}{dsdt} - \frac{d^2\overline{\Gamma}}{dsdt}\right). \tag{5}$$

Here, $\overline{\Gamma}$ refers to the decay rate of the CP-conjugated mode.

B. Weak effective Lagrangian

The effective weak Lagrangian for $c \to u\gamma$ processes can be written as [13]

$$\mathcal{L}_{\text{eff}} = \frac{4G_F}{\sqrt{2}} \left(\sum_{q,q' \in \{d,s\}} V_{cq}^* V_{uq'} \sum_{i=1}^{2} C_i O_i^{(q,q')} + \sum_{i=3}^{6} C_i O_i + \sum_{i=7}^{8} \left(C_i O_i + C_i' O_i' \right) \right) , \tag{6}$$

where G_F is Fermi's constant and V_{ij} are elements of the Cabibbo-Kobayashi-Maskawa (CKM) matrix. For the purpose of this work only the operators

$$\begin{aligned} O_1^{(q,q')} &= \left(\overline{u}_L \gamma_\mu T^a q_L'\right) \left(\overline{q}_L \gamma^\mu T^a c_L\right) , \quad & O_2^{(q,q')} &= \left(\overline{u}_L \gamma_\mu q_L'\right) \left(\overline{q}_L \gamma^\mu c_L\right) , \\ O_7 &= \frac{e m_c}{16\pi^2} \left(\overline{u}_L \sigma^{\mu\nu} c_R\right) F_{\mu\nu} , & O_7' &= \frac{e m_c}{16\pi^2} \left(\overline{u}_R \sigma^{\mu\nu} c_L\right) F_{\mu\nu} \end{aligned} \tag{7}$$

are relevant. Here, the subscripts $L(R)$ denote left-(right-)handed quark fields, T^a are generators of $SU(3)$ normalized to $\text{Tr}\{T^a T^b\} = \delta^{ab}/2$ and $F_{\mu\nu}$ is the photon field strength tensor, respectively. For $\mu_c \in \left[m_c/\sqrt{2}, \sqrt{2} m_c\right]$, the leading order Wilson Coefficients of the four quark operators $O_{1,2}^{(q,q')}$ are given by [13]

$$C_1 \in [-1.28, -0.83] , \qquad C_2 \in [1.14, 1.06] . \tag{8}$$

Within the SM, $C_{3-8}^{(\prime)}$ can be neglected due to the efficient GIM cancellation. However, we also consider BSM contributions to $C_7^{(\prime)}$ in section IV.

C. QCD frameworks for $D \to PP\gamma$ decays

In the following we use QCDF, Low's Theorem and HHχPT as QCD frameworks. We refrain from a detailed introduction of the individual models at this point. Instead, we refer to the literature cited below, as well as [10] where we provide further information on kinematics, the models and our notation.

The leading weak annihilation contribution ($\mathcal{O}(\alpha_s^0(\Lambda_{\text{QCD}}/m_c)^1)$) can be determined with QCDF methods [14–16] as

$$\begin{aligned} \mathcal{A}_-^{\text{WA}} &= i \frac{G_F e}{\sqrt{2}} C_2 \frac{f_{D_{(s)}} Q_d}{\lambda_{D_{(s)}} (v \cdot k)} \sum_{q \in \{d,s\}} V_{cd(s)}^* V_{uq} f_{(q)}^{P_1 P_2}(s) , \\ \mathcal{A}_+^{\text{WA}} &= \frac{G_F e}{\sqrt{2}} C_2 \frac{f_{D_{(s)}} Q_d}{\lambda_{D_{(s)}} (v \cdot k)} \sum_{q \in \{d,s\}} V_{cd(s)}^* V_{uq} f_{(q)}^{P_1 P_2}(s) . \end{aligned} \tag{9}$$

Here, Q_d is the electric charge of the down-type quarks and $\lambda_{D_{(s)}}$ is a non perturbative parameter of $\mathcal{O}(\Lambda_{\rm QCD})$ which is poorly known. Furthermore, $v^\mu = P^\mu/m_D$ is the four-velocity of the $D^+_{(s)}$ meson. Note that unlike the decays of the neutral D meson, the amplitudes (9) do not depend on the color-suppressed combination of the Wilson coefficients [10, 13]. Therefore, the scale uncertainty is significantly smaller. For $f_{(q)}^{P_1P_2}$ we use the electromagnetic pion and kaon form factors [17], form factors extracted from $\tau^- \to \nu_\tau K_S \pi^-$ decays [18] and isospin relations

$$\begin{aligned}
f_{(d)}^{\pi^+\pi^0}(s) &= -\sqrt{2}F^{\rm em}(s)\,,\\
f_{(d)}^{K^+\overline{K}^0}(s) &= 2F_{K^+}^{(I=1)}(s)\,,\\
f_{(s)}^{\pi^+K^0}(s) &= f_+^{\overline{K}\pi^-}(s)\,,\\
f_{(s)}^{K^+\pi^0}(s) &= -\frac{1}{\sqrt{2}} f_+^{\overline{K}\pi^-}(s)\,.
\end{aligned} \tag{10}$$

Detailed information on the form factors can also be found in appendix B1 of [10]. Note that QCDF is only applicable for small invariant masses $s \lesssim 1.5\text{GeV}^2$ of the hadronic system in the final state. We remark that there are no weak annihilation contributions for $D^+ \to \pi^+\overline{K}^0\gamma$ and $D_s \to K^+K^0\gamma$.

Low's theorem [19] relates the bremsstrahlungsamplitude of the radiative three-body decays to the amplitudes of the hadronic two-body decays

$$\mathcal{A}_-^{\rm Low} = -\frac{e\mathcal{A}(D^+_{(s)} \to P_1^+ P_2^0)}{(p_1\cdot k)(P\cdot k)}\,, \qquad \mathcal{A}_+^{\rm Low} = 0\,. \tag{11}$$

This approach is valid for soft photons with an energy below $m^2_{P^+}/E_{P^+}$ [20] and thus describes the opposite part of the phase space compared to QCDF. We don't rely on a theory prediction for $\mathcal{A}(D^+_{(s)} \to P^+P^0)$, but extract the modulus from data on branching ratios [21]. We obtain

$$\begin{aligned}
&\left|\mathcal{A}(D^+ \to \pi^+\pi^0)\right| = (2.74 \pm 0.04)\cdot 10^{-7}\,\text{GeV}\,, && \left|\mathcal{A}(D_s \to \pi^+\pi^0)\right| < 2.11\cdot 10^{-7}\,\text{GeV}\,,\\
&\left|\mathcal{A}(D^+ \to \pi^+K^0)\right| < 4.70\cdot 10^{-8}\,\text{GeV}\,, && \left|\mathcal{A}(D_s \to \pi^+K^0)\right| = (5.75 \pm 0.12)\cdot 10^{-7}\,\text{GeV}\,,\\
&\left|\mathcal{A}(D^+ \to K^+\pi^0)\right| = (1.16 \pm 0.06)\cdot 10^{-7}\,\text{GeV}\,, && \left|\mathcal{A}(D_s \to K^+\pi^0)\right| = (2.9 \pm 0.5)\cdot 10^{-7}\,\text{GeV}\,,\\
&\left|\mathcal{A}(D^+ \to K^+\overline{K}^0)\right| = (6.62 \pm 0.10)\cdot 10^{-7}\,\text{GeV}\,, && \left|\mathcal{A}(D_s \to K^+\overline{K}^0)\right| = (2.10 \pm 0.05)\cdot 10^{-6}\,\text{GeV}\,,\\
&\left|\mathcal{A}(D^+ \to \pi^+\overline{K}^0)\right| = (1.396 \pm 0.014)\cdot 10^{-6}\,\text{GeV} && \left|\mathcal{A}(D_s \to K^+K^0)\right| < 5.36\cdot 10^{-8}\,\text{GeV}\,.
\end{aligned} \tag{12}$$

Note that there is only an upper limit on the $D_s \to \pi^+\pi^0$ branching ratio. We remark that it turns out that HHχPT implies an amplitude about two orders of magnitude smaller. Moreover, in the isospin limit, the amplitude vanishes. Furthermore, for the decays into neutral kaons, only the branching ratio of $D_s \to K^+\overline{K}^0$ is measured. We extract the corresponding amplitudes for the remaining decays from data for final states with K_S and K_L. This procedure leads to huge

uncertainties for the DCS decays. Therefore, we only give upper limits for these amplitudes. All upper limits refer to a 90% confidence level. As it is sizable we explicitly take the uncertainty of the $D_s \to K^+\pi^0$ amplitude in our numerical analysis into account, but neglect the uncertainties in (12) from the other decay channels.

Furthermore, we employ HHχPT [22–24] extended by light vector resonances [25]. The parity-even and parity-odd amplitudes are given in terms of form factors $A_i^{(q,q')}, B_i^{(q,q')}, D_i^{(q,q')}$ and $E_i^{(q,q')}$

$$\begin{aligned} A_-^{\mathrm{HH}\chi\mathrm{PT}} &= \frac{G_F e}{\sqrt{2}} \sum_{q,q'\in\{d,s\}} V_{cq}^* V_{uq'} \left[(C_2 - \frac{1}{6} C_1) \sum_i A_i^{(q,q')} + \frac{1}{2} C_1 \sum_i E_i^{(q,q')} \right] , \\ A_+^{\mathrm{HH}\chi\mathrm{PT}} &= \frac{G_F e}{\sqrt{2}} \sum_{q,q'\in\{d,s\}} V_{cq}^* V_{uq'} \left[(C_2 - \frac{1}{6} C_1) \sum_i B_i^{(q,q')} + \frac{1}{2} C_1 \sum_i D_i^{(q,q')} \right] . \end{aligned} \tag{13}$$

In Appendix A the corresponding diagrams are shown in Fig. 10 to 20 and the non-zero contributions to the form factors are listed. We consider the masses of the light pseudoscalars only in phase space and in their propagators. Otherwise we neglect them in the form factors. To enforce Low's theorem, we remove the bremsstrahlung contributions $A_{1,2,3}$ and $E_{1,2}$ in (13) and add (11) while using the strong and weak phases predicted by HHχPT. For the diagrams $A_{6,1}$, the contributions of longitudinal polarization of the $D_{(s)}^+ \to V^+V^0$ subdiagram have to be removed in order to obtain a gauge invariant amplitude [26].

III. SM PREDICTIONS

In this section we compare SM predictions for the branching ratios (Section III A) and forward-backward asymmetries (Section III B) of the QCD frameworks given in Sec. II C. SM CP asymmetries are discussed in Section III C.

A. Branching ratios

The Dalitz plots in Fig. 1 illustrate the SM predictions based on HHχPT. The bands in s, t and u, which are generated by the intermediate ρ, ω and $K^\star$ resonances, are particularly distinctive. Furthermore, the significant bremsstrahlung effects can be seen for large s. For the decays $D_{(s)}^+ \to K^+\overline{K}^0\gamma$ $D^+ \to \pi^+\overline{K}^0\gamma$ and $D_s \to K^+K^0\gamma$, a preference of the u-channel resonance over the t-channel resonance is observed. This is due to constructive interference of the u-channel contributions from the form factors B and D, while the t-channel contributions interfere destructively.

Figure 2 shows the differential branching ratios of all considered decay channels as a function of

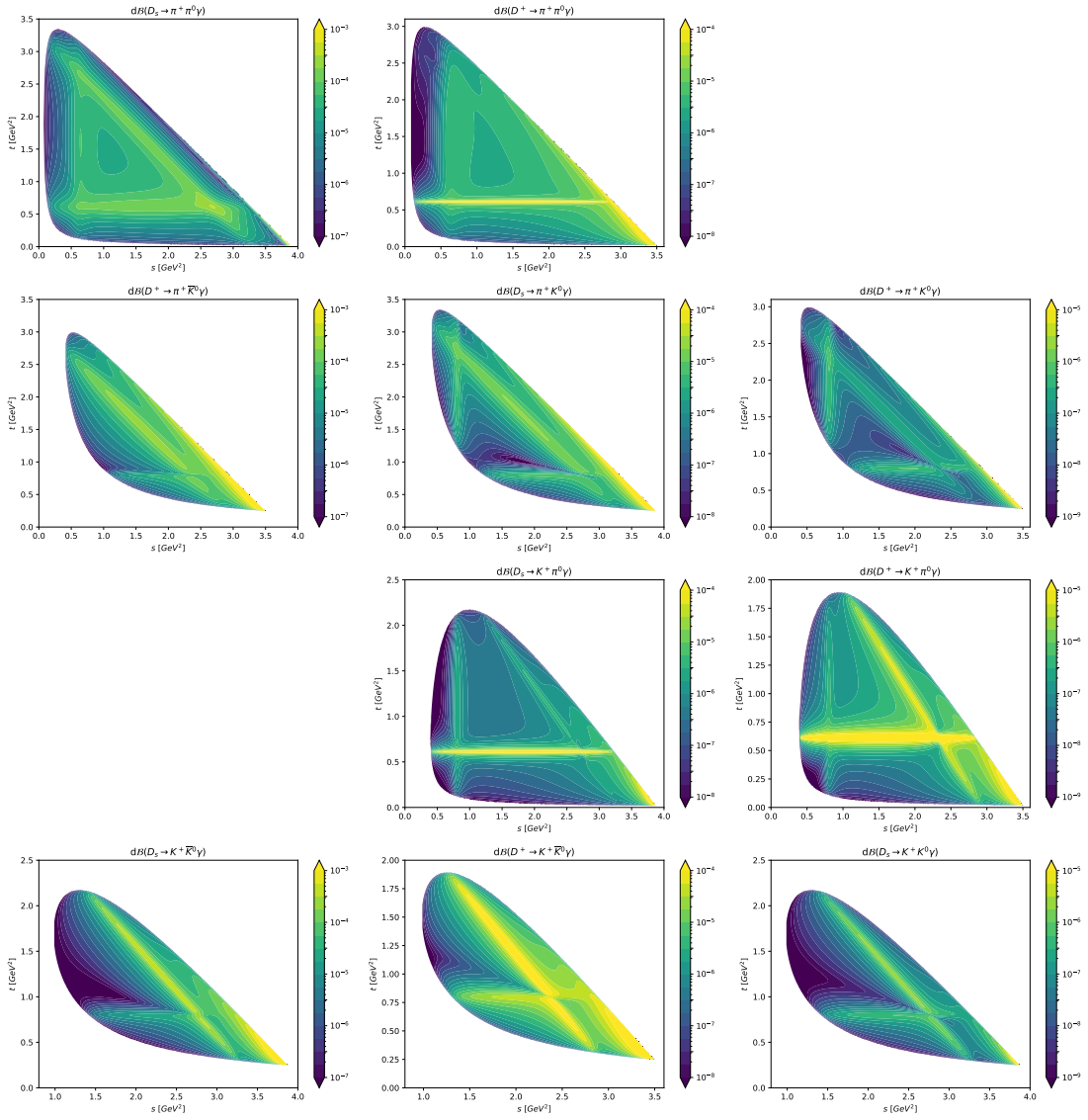

Figure 1: Dalitz plots based on the SM HHχPT predictions for $\mu_c = m_c$ and the mean value of the $D_{(s)} \to P^+P^0$ amplitude. The first, second and third columns show the CF, SCS and DCS decay modes, respectively. Each row shows the same final state or the final state with $K^0 \leftrightarrow \overline{K}^0$.

s. For each decay, the predictions of QCDF (blue), HHχPT (green) and Low's Theorem (red) are illustrated. The width of the bands arise from the μ_c dependence of the Wilson Coefficients and the uncertainty on the $D_s \to K^+\pi^0$ amplitude.

The distinct resonance in the QCDF results is a consequence of the $P^+ - P^0$ form factors dominating the shape of the distributions. For the final state $K^+K\gamma$ no resonance peak can be identified, since the lowest ρ resonance is outside of the phase space. In comparison, the s-channel resonances in the HHχPT predictions only result in a distinct peak for the final state $\pi^+K^0\gamma$.

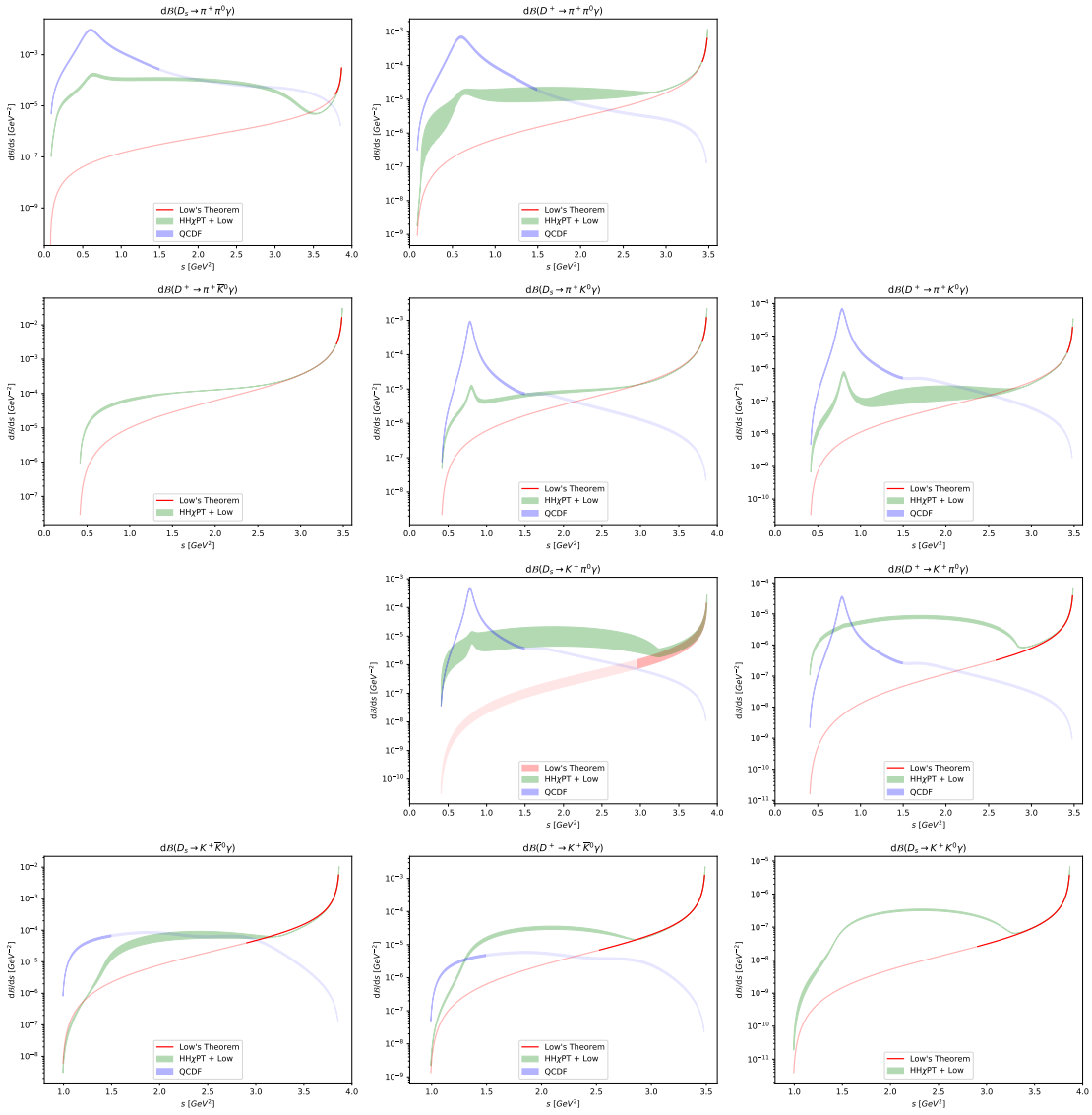

Figure 2: Single differential branching ratios based on Low's Theorem (red), HHχPT (green) and QCDF (blue) within the SM. The darker shaded areas and lines correspond to the model's region of applicability. QCDF predictions are obtained for $\lambda_{D_{(s)}} = 0.1\,\text{GeV}$ and scale with $(0.1\,\text{GeV}/\lambda_{D_{(s)}})^2$. The first, second and third columns show the CF, SCS and DCS decay modes, respectively. Each row shows the same final state or the final state with $K^0 \leftrightarrow \overline{K}^0$.

The other decays are mostly dominated by the t- and u-channel resonances in the range of small and intermediate values of s. In particular, the contributions of the ω resonances are large due to the significant $\omega\pi\gamma$ coupling. For large s, the bremsstrahlung is dominating and the results are approaching to those of Low's theorem due to the replacement of the model's own bremsstrahlung contribution.

In Table I and II we give the branching ratios for the SM-like decay modes. The QCDF results

	$D_s \to \pi^+\pi^0\gamma$	$D^+ \to \pi^+\overline{K}^0\gamma$	$D_s \to K^+\overline{K}^0\gamma$
$\text{QCDF}\big\vert^{\text{SM}}_{s\leq 1.5\ \text{GeV}^2}$	$(2.8-3.2)\cdot 10^{-3}$	–	$(1.8-2.1)\cdot 10^{-5}$
$\text{HH}\chi\text{PT}\big\vert^{\text{SM}}_{s\leq 1.5\ \text{GeV}^2}$	$(1.1-1.5)\cdot 10^{-4}$	$(6.0-6.7)\cdot 10^{-5}$	$(2.5-3.2)\cdot 10^{-6}$
$\text{HH}\chi\text{PT}\big\vert^{\text{SM}}_{E_\gamma\geq 0.1\ \text{GeV}}$	$(2.4-3.0)\cdot 10^{-4}$	$(3.5-3.6)\cdot 10^{-4}$	$(1.5-2.0)\cdot 10^{-4}$

Table I: Branching ratios for the CF decays. The branching ratios are given in the region of applicability of QCDF $s \lesssim 1.5\,\text{GeV}^2$ for QCDF and HHχPT to enable a comparison of both models. Additionally, HHχPT predictions are given for $E_\gamma \geq 0.1\,\text{GeV}$, see text for details. The QCDF branching ratios are obtained for $\lambda_{D_{(s)}} = 0.1\,\text{GeV}$ and are $\propto (0.1\,\text{GeV}/\lambda_{D_{(s)}})^2$.

	$D^+ \to \pi^+K^0\gamma$	$D^+ \to K^+\pi^0\gamma$	$D_s \to K^+K^0\gamma$
$\text{QCDF}\big\vert^{\text{SM}}_{s\leq 1.5\ \text{GeV}^2}$	$(7.2-8.3)\cdot 10^{-6}$	$(3.7-4.3)\cdot 10^{-6}$	–
$\text{HH}\chi\text{PT}\big\vert^{\text{SM}}_{s\leq 1.5\ \text{GeV}^2}$	$(1.2-2.0)\cdot 10^{-7}$	$(4.5-5.8)\cdot 10^{-6}$	$(7-8)\cdot 10^{-9}$
$\text{HH}\chi\text{PT}\big\vert^{\text{SM}}_{E_\gamma\geq 0.1\ \text{GeV}}$	$(3.9-6.6)\cdot 10^{-7}$	$(1.2-1.5)\cdot 10^{-5}$	$(4.3-4.7)\cdot 10^{-7}$

Table II: As in Table I but for the DCS decay modes.

only include the phase space up to $s \leq 1.5\text{GeV}$. For comparison, we show the HHχPT branching ratios for this cut as well. Furthermore, we employ the phase space cut $E_\gamma \geq 0.1\text{GeV}$ to avoid the soft photon pole, where $E_\gamma = (m_D^2 - s)/(2m_D)$ is the photon energy in the $D^+_{(s)}$ meson's rest frame. QCDF leads to larger values for the decays $D_s \to \pi^+\pi^0\gamma$, $D_s^+ \to K^+\overline{K}^0\gamma$ and $D^+ \to \pi^+K^0\gamma$ as a result of the large s-channel contributions and the small value of $\lambda_{D_{(s)}}$. We note that the branching ratio of $D_s^+ \to K^+\overline{K}^0\gamma$ is about two orders of magnitude smaller than the one of $D_s \to \pi^+\pi^0\gamma$, although both decays are CF, since the lightest ρ is not inside the phase space of $D_s^+ \to K^+\overline{K}^0\gamma$. Due to the missing t- and u-channel resonances in QCDF and the large $\omega\pi\gamma$ coupling, HHχPT predicts larger branching ratios for $D^+ \to K^+\pi^0\gamma$. SM branching ratios for the SCS modes are given in Table III.

B. Forward-Backward Asymmetry

Angular observables are also suitable for testing QCD models. Here we study $A_{\text{FB}}(s)$ as defined in (4). Within the SM, QCDF predicts $A_{\text{FB}}(s) = 0$ since the amplitudes depend only on s (and not on t, u). The SM forward-backward asymmetry based on HHχPT is shown in Fig. 3. We illustrate $A_{\text{FB}}(s)$ without contributions from resonances (red), only with individual resonances and

the complete results (dark blue). The forward-backward asymmetry is dominated by resonances in the region of small and intermediate s. The effect of the ω is particularly large as can be seen for the decays $D^+ \to \pi^+\pi^0\gamma$ and $D^+_{(s)} \to K^+\pi^0\gamma$. The decay $D_s \to \pi^+\pi^0\gamma$ has no contribution from the ω despite the π^0 in the final state. The effects of the ρ^+ and ρ^0 cancel almost exactly. Deviations from $A_{\rm FB}(s) = 0$ originate from the small difference in the $\rho^0\pi^0\gamma$ and $\rho^+\pi^+\gamma$ coupling and from the non-resonant contributions. Since the s-channel resonances only generate dependencies on s, they can significantly reduce the asymmetry at the $(P^+P^0)_{\rm res}$ peak for some decay channels. In some cases, however, the interference term can even increase the asymmetry. There are no s-channel resonances for $D^+ \to \pi^+\overline{K}^0\gamma$ and $D_s \to K^+K^0\gamma$. The corresponding plots are therefore identical to the non-resonant case. For the decays $D^+ \to \pi^+\overline{K}^0\gamma$, $D_s \to K^+\overline{K}^0\gamma$, $D^+ \to \pi^+\pi^0\gamma$ and $D^+ \to \pi^+K^0\gamma$ significant scale uncertainties arise for the t-channel contribution due to the interference of the form factors B and D. Since the t-channel resonances provide the only large contribution in the forward region for small and intermediate s, this uncertainty is clearly visible in the plots. In the high s region, the forward-backward asymmetry is dominated by the bremsstrahlung. Complementary to the $D^0 \to P^+P^-\gamma$ decays [10], the bremsstrahlung of the $D^+_{(s)}$ decays always results in a large asymmetry, since one of the final state mesons is uncharged and thus cannot emit a photon.

C. SM CP Asymmetries

Within the SM, QCDF at leading order implies a vanishing CP asymmetry since the WA amplitude contains only one weak phase. On the other hand, HHχPT predicts non-zero CP asymmetries for the SCS modes $D^+ \to K^+\overline{K}^0\gamma$, $D_s \to K^+\pi^0\gamma$ and $D_s \to \pi^+K^0\gamma$ as shown in the Dalitz plots in Fig. 4. For the first two decays, it can be seen that there are large cancellations when integrating over t. This leads to rather small single-differential CP-asymmetries of $|A_{\rm CP}(s)| \lesssim 1.8 \cdot 10^{-5}$ and $|A_{\rm CP}(s)| \lesssim 4.5 \cdot 10^{-5}$, respectively. For $D_s \to \pi^+K^0\gamma$, there are also cancellations between the t- and u-channel resonance. However, significantly larger values of $|A_{\rm CP}(s)| \lesssim 2.5 \cdot 10^{-4}$ can be seen at the $(P^+P^0)_{\rm res}$ peak. The SM CP asymmetry for $D^+ \to \pi^+\pi^0\gamma$ vanishes in the isospin limit. The CP asymmtries of the CF and DCS modes vanish as there is only one weak (CKM) phase involved.

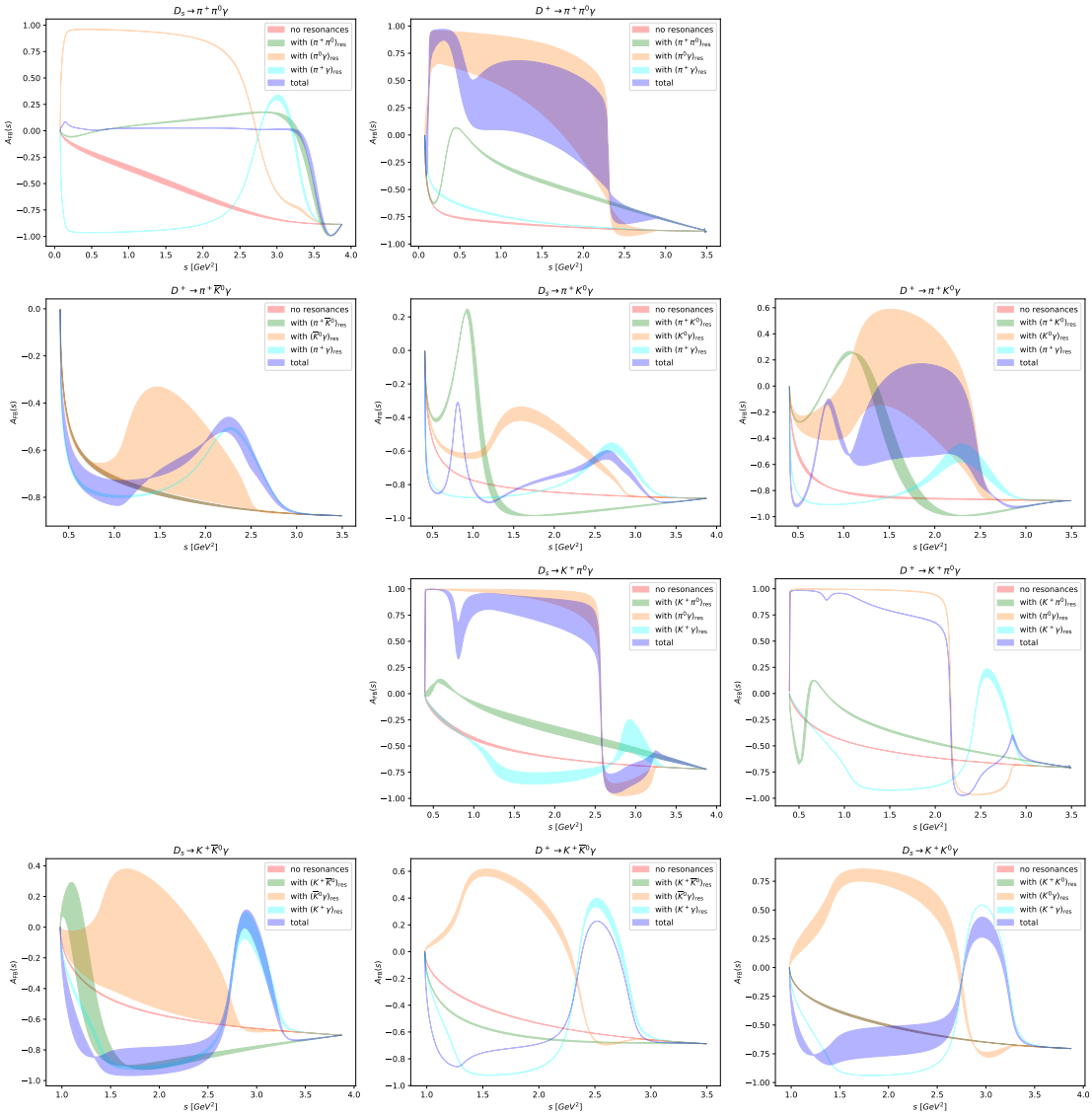

Figure 3: The SM forward backward asymmetry $A_{\rm FB}(s)$ (4) as a function of s based on HHχPT. Purely non-resonant contributions are shown by the red bands. The green, orange and light blue bands contain additional contributions of a specific resonance channel. The dark blue bands represent the complete FB asymmetries. $A_{\rm FB}^{\rm SM}(s)$ vanishes for the leading order QCDF contribution. The first, second and third columns show the CF, SCS and DCS decay modes, respectively. Each row shows the same final state or the final state with $K^0 \leftrightarrow \overline{K}^0$.

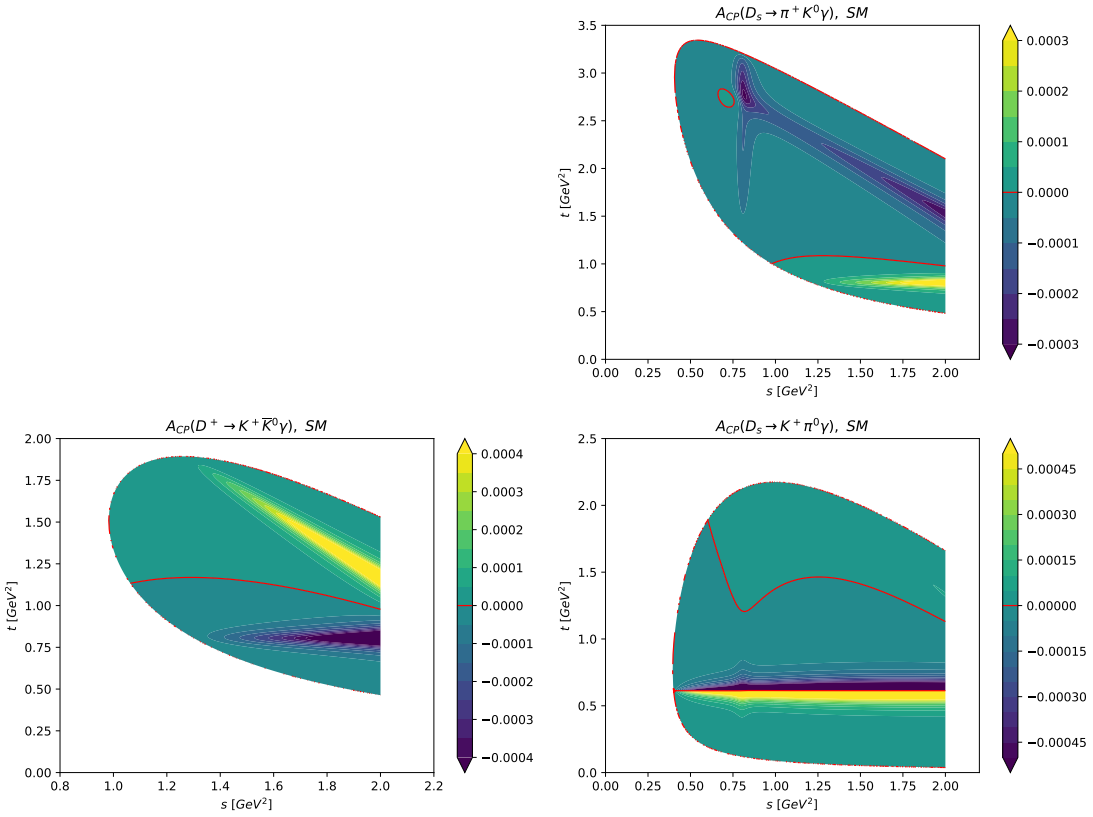

Figure 4: Dalitz plot of $A_{\rm CP}(s,t)$ for $D_s \to \pi^+ K^0 \gamma$ (upper right), $D^+ \to K^+ \overline{K}^0 \gamma$ (lower left) and $D_s \to K^+ \pi^0 \gamma$ (lower right) based on HHχPT within the SM. We employed a cut $s \leq 2\,\text{GeV}^2$ to avoid large bremsstrahlung contributions in the normalization. $A_{\rm CP}^{\rm SM}(s,t)$ vanishes for $D^+ \to \pi^+ \pi^0 \gamma$ and is therefore not shown as the CP asymmetries of the CF and DCS modes.

IV. BSM SIGNATURES

We study the impact of BSM physics for the SCS decays. We consider contributions of the electromagnetic dipole operators

$$\begin{aligned} \mathcal{A}_-^{\rm BSM} &= i\frac{G_F e}{\sqrt{2}}\frac{m_c}{4\pi^2}(C_7 + C_7')\frac{(b'-a')}{v\cdot k}\,, \\ \mathcal{A}_+^{\rm BSM} &= \frac{G_F e}{\sqrt{2}}\frac{m_c m_D}{2\pi^2}(C_7 - C_7')h'\,. \end{aligned} \tag{14}$$

Corresponding contributions within the SM can be neglected due to the strongly suppressed Wilson coefficients. On the other hand, $C_7^{(\prime)}$ can reach $\mathcal{O}(0.1)$ values through BSM physics. Model-independent analyses of $D \to \rho^0 \gamma$ and $D \to \pi \ell \ell$ decays yield the constraints [6, 7, 27]

$$|C_7|, |C_7'| \lesssim 0.3\,. \tag{15}$$

The tensor current form factors a', b', c' and h' are defined in appendix A.

In the following we discuss the NP impact on branching ratios (Sec. IV A), the forward-backward asymmetry (Sec. IV B) and the CP-asymmetry (Sec. IV C).

A. BSM effects in the branching ratios

In Fig. 5 we show a comparison of SM predictions (blue) and different BSM scenarios of the FCNC modes based on HHχPT. We set one of the BSM coefficients $C_7^{(\prime)}$ to zero and exhaust the limit (15) of the other one. The CP-phases are set to $0, \pm\pi/2, \pi$. The differential branching ratios can be increased by one order of magnitude at the s-channel peak. As noted previously, the decay $D_s \to K^+\overline{K}^0\gamma$ is an exception. Since the ρ^+ resonance is outside of the phase space, the BSM contributions are negligibly small in the entire phase space. For QCDF, the largest deviation between SM and BSM scenarios arise above the s-channel peak. The deviations are below one order of magnitude for $\lambda_{D_{(s)}} = 0.1$GeV. At the s-channel peak, the deviations are significantly smaller. Especially for $C_7' = 0$, the SM predictions and BSM scenarios hardly differ from each other. Since the deviations between SM and BSM are not very large and sizable t- and u-channel contributions are to be expected beyond the s-channel peak, which are not taken into account in leading order QCDF, we do not show plots of differential branching ratios within QCDF. In Table III we give (integrated) branching ratios within QCDF and HHχPT for the FCNC modes. We employ the same phase space cuts as in Table I. We conclude that the (differential) branching ratios of SCS decays are affected by BSM physics, however, are not sufficiently clean to unambiguously signal NP.

B. BSM effects in $A_{\rm FB}$

We investigate $A_{\rm FB}$ based on HHχPT in Fig. 6 in the same BSM scenarios as those considered in Sec. IV A. Since the dipole operators $O_7^{(\prime)}$ induce a t-dependence only by non-resonant contributions, there are only small forward-backward asymmetries for SM QCDF contributions. For $\lambda_{D_{(s)}} = 0.1\,\text{GeV}$, $A_{\rm FB}(s)$ reach values of $\mathcal{O}(10^{-3}) - \mathcal{O}(10^{-2})$. For $\lambda_{D_{(s)}} = 0.3\,\text{GeV}$, the SM contribution is significantly reduced, leading to larger asymmetries. These are typically in the range of $\mathcal{O}(10^{-2})$, but can occasionally reach larger values of $|A_{\rm FB}(s)| \lesssim 0.15$. The minor t-dependence of the BSM contributions can lead to a significant suppression of the substantial SM asymmetries predicted by HHχPT. These are considerably reduced, especially in the region of the s-channel resonance. This becomes particularly evident in case of $D^+ \to \pi^+\pi^0\gamma$.

Similarly to the decays of neutral D mesons, sizable effects of the dipole operators can be seen

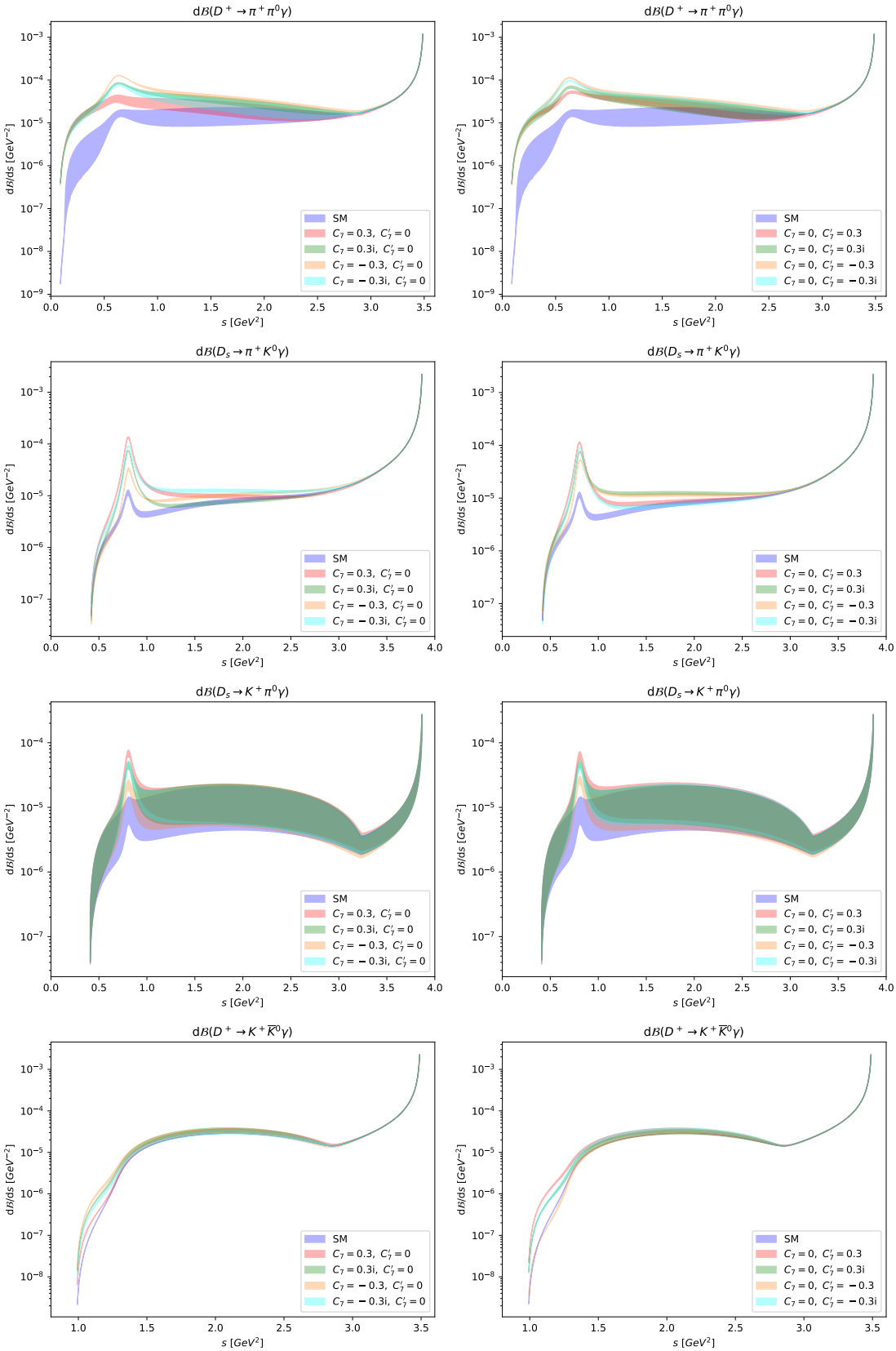

Figure 5: Differential branching ratios for several BSM scenarios based on HHχPT. We exhaust the limit of one BSM coefficient (15) and set the other one to zero. We overlay distributions obtained for CP-phases set to $0, \pm\pi/2$ and π.

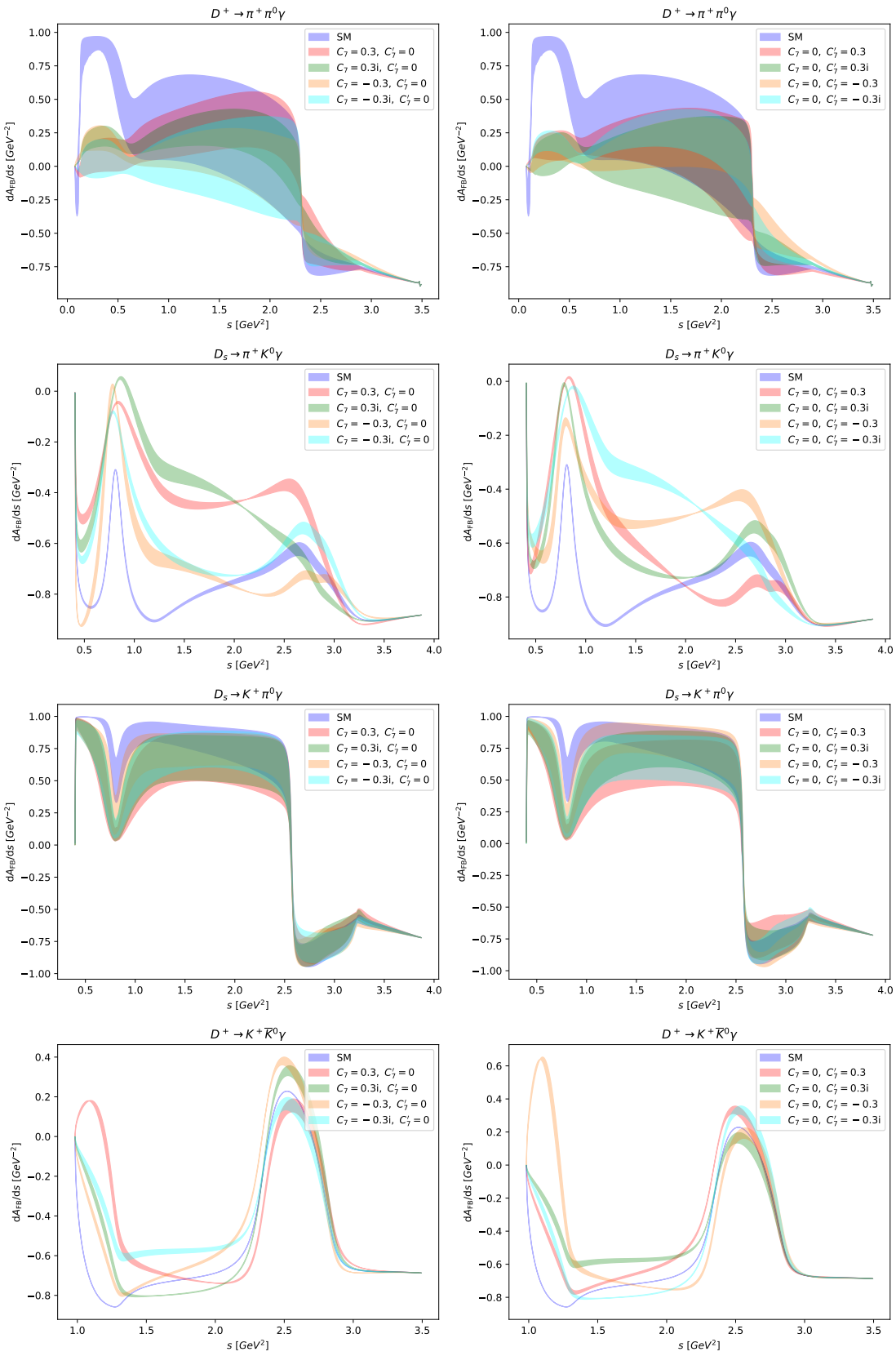

Figure 6: A comparison of SM and BSM FB asymmetries based on HHχPT. We show the same BSM scenarios as for the branching ratios in Fig. 5

	$D^+ \to \pi^+\pi^0\gamma$	$D_s \to \pi^+ K^0\gamma$	$D_s \to K^+\pi^0\gamma$	$D^+ \to K^+\overline{K}^0\gamma$
$\text{QCDF}\big\vert^{\text{SM}}_{s\leq 1.5\ \text{GeV}^2}$	$(2.1-2.4)\cdot 10^{-4}$	$(0.9-1.1)\cdot 10^{-4}$	$(5.0-5.8)\cdot 10^{-5}$	$(1.3-1.5)\cdot 10^{-6}$
$\text{HH}\chi\text{PT}\big\vert^{\text{SM}}_{s\leq 1.5\ \text{GeV}^2}$	$(1.0-2.2)\cdot 10^{-5}$	$(4.4-5.5)\cdot 10^{-6}$	$(0.3-1.4)\cdot 10^{-5}$	$(1.8-2.3)\cdot 10^{-6}$
$\text{HH}\chi\text{PT}\big\vert^{\text{SM}}_{E_\gamma\geq 0.1\ \text{GeV}}$	$(3.0-5.4)\cdot 10^{-5}$	$(2.8-3.1)\cdot 10^{-5}$	$(1.0-4.3)\cdot 10^{-5}$	$(3.8-4.6)\cdot 10^{-5}$
$\text{QCDF}\big\vert^{\text{BSM}}_{s\leq 1.5\ \text{GeV}^2}$	$(1.2-4.0)\cdot 10^{-4}$	$(0.5-1.8)\cdot 10^{-4}$	$(2.7-9.5)\cdot 10^{-5}$	$(0.5-3.1)\cdot 10^{-6}$
$\text{HH}\chi\text{PT}\big\vert^{\text{BSM}}_{s\leq 1.5\ \text{GeV}^2}$	$(2.7-7.7)\cdot 10^{-5}$	$(0.9-2.3)\cdot 10^{-5}$	$(0.5-2.3)\cdot 10^{-5}$	$(1.6-3.1)\cdot 10^{-6}$
$\text{HH}\chi\text{PT}\big\vert^{\text{BSM}}_{E_\gamma\geq 0.1\ \text{GeV}}$	$(0.5-1.3)\cdot 10^{-4}$	$(3.5-5.0)\cdot 10^{-5}$	$(1.3-5.5)\cdot 10^{-5}$	$(3.7-5.0)\cdot 10^{-5}$

Table III: Branching ratios for the BSM sensitive SCS decays in the SM (top entries) and with BSM physics (lower entries). For the BSM branching ratios, we employed the same general scenarios as for Fig. 5. The branching ratios are given in the region of applicability of QCDF $s \lesssim 1.5\,\text{GeV}^2$ for QCDF and HHχPT to enable a comparison of both models. Additionally, HHχPT predictions are given for $E_\gamma \geq 0.1\,\text{GeV}$, see text for details. The QCDF branching ratios are obtained for $\lambda_{D_{(s)}} = 0.1\,\text{GeV}$ and are $\propto (0.1\,\text{GeV}/\lambda_{D_{(s)}})^2$ in the SM.

for differential branching ratios and forward backward asymmetries [10]. However, it is difficult to claim sensitivity to NP due to the uncertainties of the leading order calculation and the intrinsic uncertainty of the Breit-Wigner contributions. Nevertheless, these observables are suitable for testing the various QCD models with SM-like decays and for understanding the decay mechanisms. Due to the small CP-violating phases in the charm sector of the SM, CP-asymmetries, discussed in the next section, have the best sensitivity to NP.

C. BSM CP violation

The most promissing observable to test BSM physics is the single- or double-differential CP asymmetry defined in (5). Note that we perform a cut $s \leq 2\,\text{GeV}^2$ for HHχPT to avoid large bremsstrahlung contributions in the normalization. For QCDF, we include the contributions with $s \leq 1.5\,\text{GeV}^2$.

Considering possible BSM contributions in the electromagnetic dipole operator, all FCNC decay modes can exhibit sizable CP-asymmetries. In Fig. 7 we show $A_{\text{CP}}(s)$ for different BSM scenarios. We set one of the BSM coefficients to zero and the other one to $0.05i$ or $0.2i$. To maximize $A_{\text{CP}}(s)$, we choose $C_7^{(\prime)}$ to be purely imaginary. Since the QCDF amplitude does not contain effects of the t- and u-channel resonances, significant strong phases and thus also CP asymmetry only arise

at the $(P^+P^0)_{\rm res}$ peak. Therefore, we do not show Dalitz plots for QCDF. Within these BSM scenarios, $A_{\rm CP}(s)$ can reach $\mathcal{O}(0.01)$ values for $D^+ \to K^+\overline{K}^0\gamma$ and $\mathcal{O}(0.1)$ values otherwise. The CP asymmetries for $D_s \to \pi^+K^0\gamma$ and $D_s \to K^+\pi^0\gamma$ are almost identical, since the amplitudes differ basically only by an isospin factor of $-1/\sqrt{2}$. Minor deviations are caused by different momenta in the heavy meson propagators of the tensor form factors and the different shape of the phase space.

In Fig. 8 we show Dalitz plots for the double differential CP asymmetry for HHχPT where we set one of the coefficients $C_7^{(\prime)}$ to $0.1i$. It can be seen that the values for $A_{\rm CP}(s,t)$ are increased by a factor of $\sim 10^3$ compared to the SM. Furthermore, the single differential CP asymmetries are shown in Fig. 9 for the same BSM scenarios as for QCDF. For $D^+ \to \pi^+\pi^0\gamma$ and $D_s \to K^+\pi^0\gamma$, the parity even and parity odd amplitudes contribute to the s-channel peak to the same extend. The relative sign between C_7 and C_7' in (14) results in a cancellation for C_7 and a constructive increase for C_7', respectively. This characteristic feature can also be observed in $D^0 \to \pi^+\pi^-\gamma$ [10]. In contrast, for $D_s \to \pi^+K^0\gamma$ the s-channel peak is dominated by $\mathcal{A}_-$. Complementary, the tails, generated by the t- and u-channel resonance, change sign in the two BSM scenarios. Therefore, it is dominated by $\mathcal{A}_+$. Since the t- and u-channel resonances are different vector mesons, the cancellation is not as effective as for $D^0 \to P^+P^-\gamma$ decays [10].

We stress that QCD renormalization-group evolution connects the electromagnetic and chromomagnetic dipole operators. Therefore, data on $\Delta A_{\rm CP} = A_{\rm CP}(D^0 \to K^+K^-) - A_{\rm CP}(D^0 \to \pi^+\pi^-)$ can constrain the phase of the photon dipoles as $|{\rm Im}(C_7^{(\prime)})| \lesssim 2 \cdot 10^{-3}$ in several BSM models, see [10] for further details. Since $A_{\rm CP}$ scales approximately linear with ${\rm Im}(C_7^{(\prime)})$ for $|C_7^{(\prime)}| \lesssim 0.1$ this would lead to a suppression factor of 50 relative to the asymmetries shown in Fig. 8. However, resulting CP-asymmetries reach few permille level and are more than one order of magnitude larger than the ones in the the SM.

For larger photon dipole coefficients $|C_7^{(\prime)}| \gtrsim 0.1$, the BSM contributions lead to enlarged branching ratios for $D^+ \to \pi^+\pi^0\gamma$, $D_s \to \pi^+K^0\gamma$ and $D_s \to K^+\pi^0\gamma$, as shown in Fig. 5. This corresponds to an increase of the normalization of the CP asymmetry (5). Thus, for sizable $|C_7^{(\prime)}| \gtrsim 0.1$, the CP asymmetry no longer scales linearly with ${\rm Im}(C_7^{(\prime)})$, which can also be seen for $A_{\rm CP}(s)$ in Fig. 9.

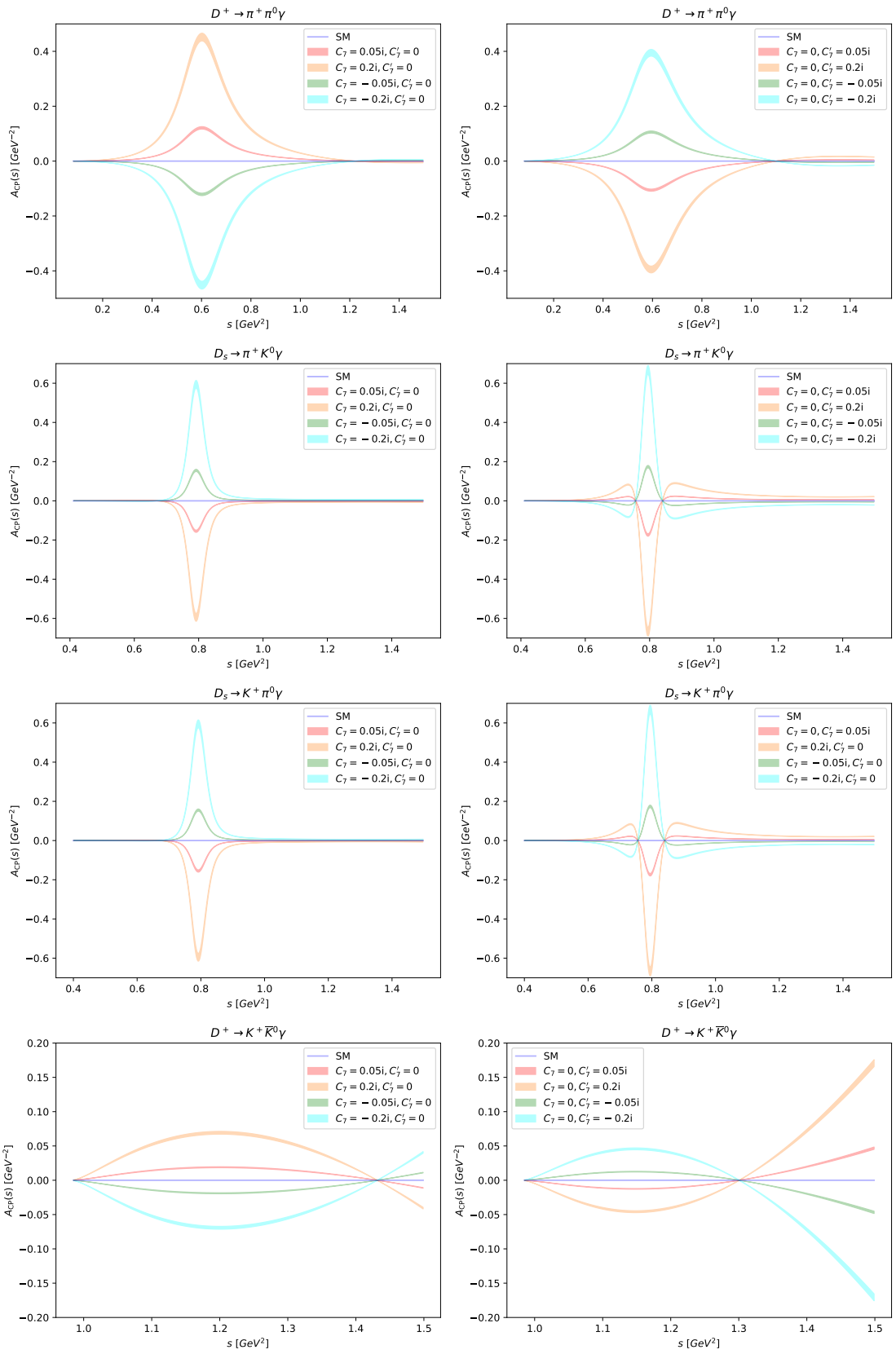

Figure 7: The CP asymmetry as a function of s, based on SM QCDF and (14). Plots in the left column correspond to $C_7 = \pm 0.05\, i$ or $\pm 0.2\, i$ and $C_7' = 0$. Plots in the right column correspond to $C_7' = \pm 0.05\, i$ or $\pm 0.2\, i$ and $C_7 = 0$. We performed a cut $s \leq 1.5\,\text{GeV}^2$ to remain within the region where QCDF applies.

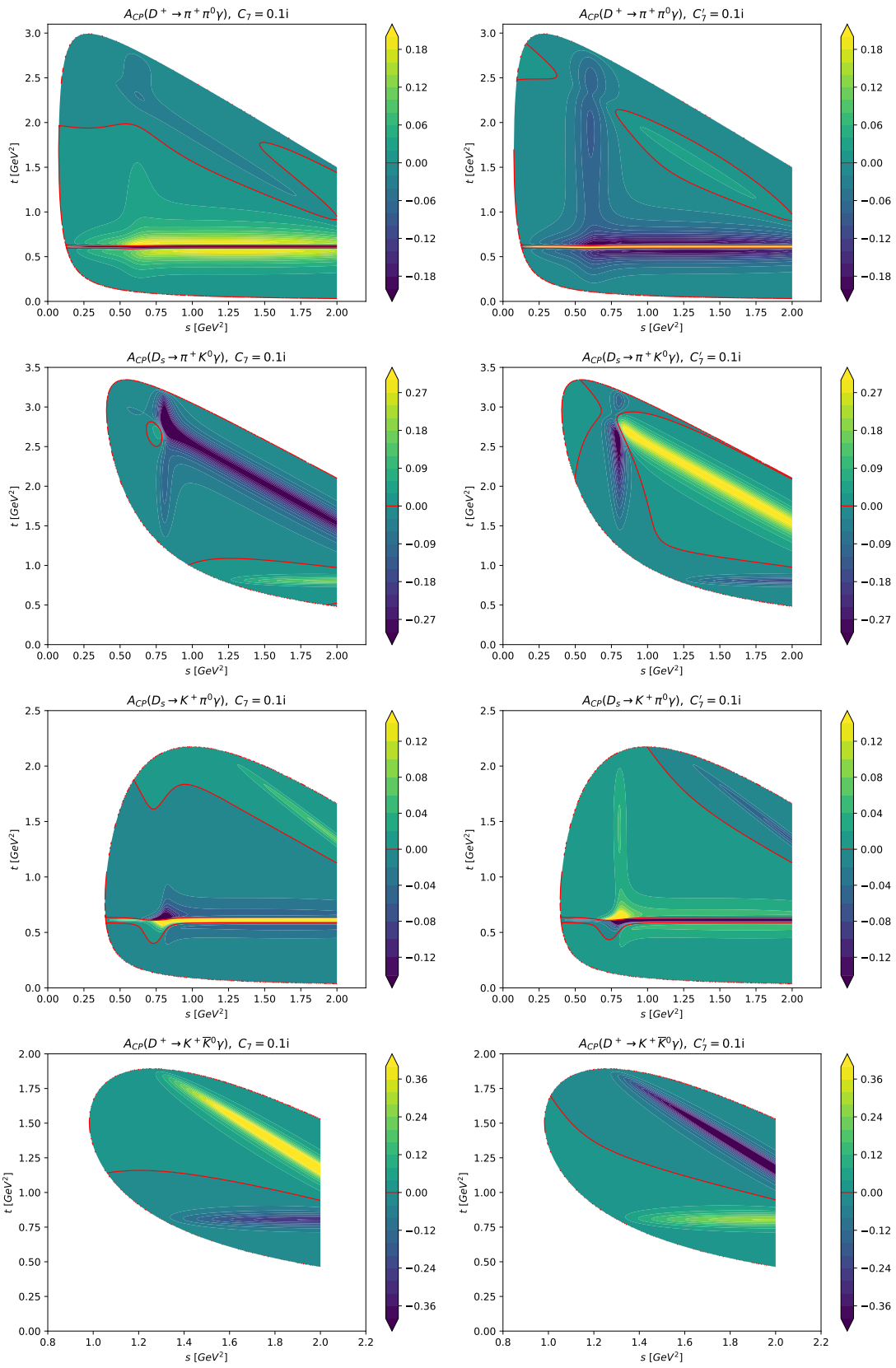

Figure 8: Dalitz plot of $A_{\rm CP}(s,t)$ for $D^+ \to \pi^+\pi^0\gamma$ (first row), $D_s \to \pi^+K^0\gamma$ (second row), $D_s \to K^+\pi^0\gamma$ (third row) and $D^+ \to K^+\overline{K}^0\gamma$ (fourth row) based on HHχPT. Plots to the left (right) correspond to $C_7 = 0.1\,i$ and $C_7' = 0$ ($C_7' = 0.1\,i$ and $C_7 = 0$). We employed a cut $s \leq 2\,\mathrm{GeV}^2$ to avoid large bremsstrahlung contributions in the normalization.

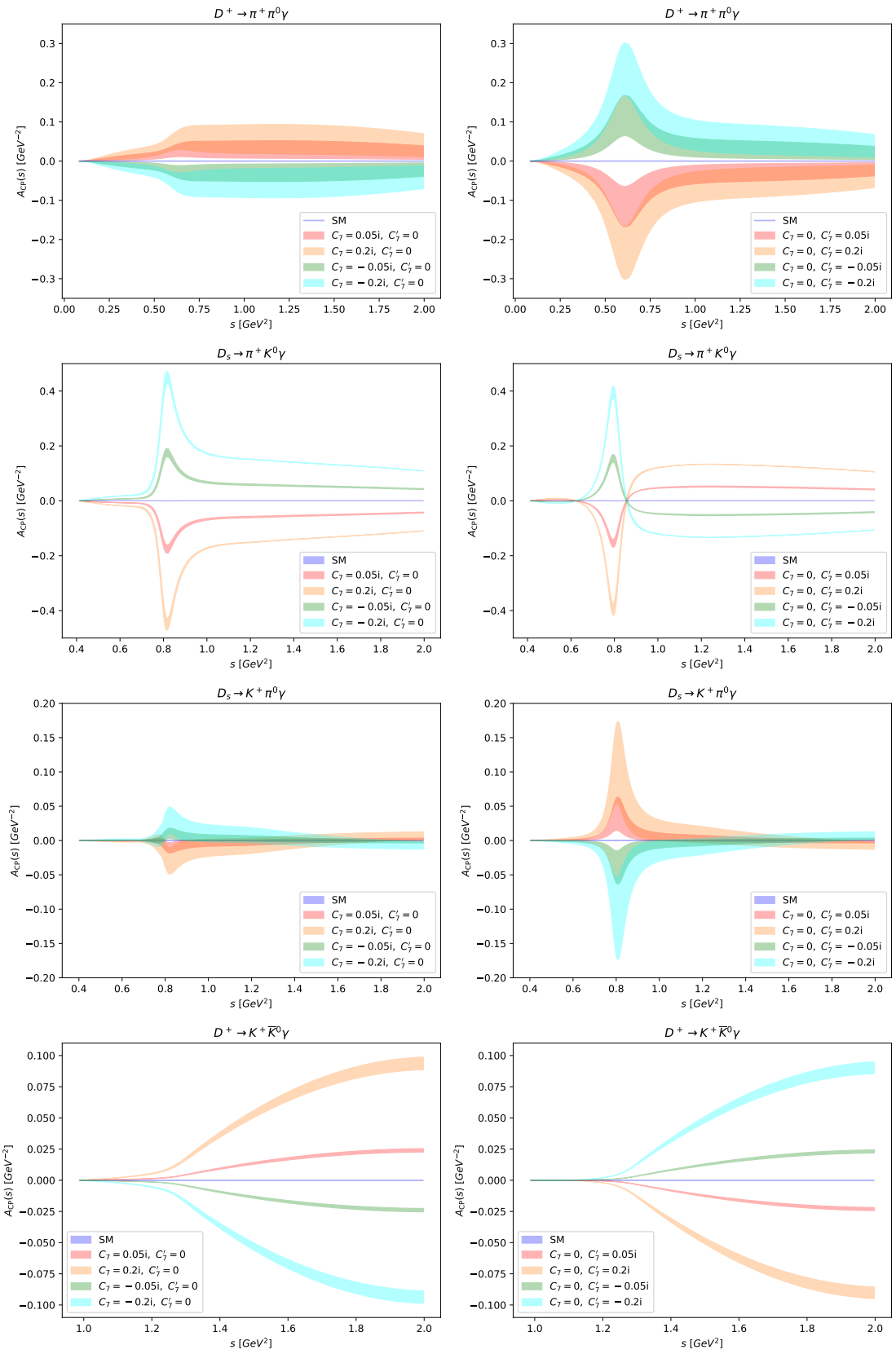

Figure 9: As in Fig. 7 but for HHχPT and with cut $s \leq 2\,\mathrm{GeV}^2$ to avoid large bremsstrahlung contributions in the normalization.

V. SUMMARY

We analyzed ten radiative three-body decays of charged, charmed mesons $D^+_{(s)} \to P^+P^0\gamma$ in the standard model and beyond. This work complements earlier works on neutral meson decays [10]. The decay amplitudes and distributions are computed in QCDF, HHχPT, and in the region of high PP-invariant mass, using the soft photon approximation. The DCS and CF modes (1) are SM-like and probe the QCD dynamics. Branching ratios are shown in Fig. 2 and compared in Table I and II. As in [10] the forward-backward asymmetry (4) is an observable that efficiently differentiates between predictions of lowest order QCDF, weak annihilation-type contributions with s-channel dependence only, and HHχPT, subject to more complex resonance structures. An understanding of the dominant decay dynamics can therefore be achieved from experimental study, and increases the sensitivity of the NP searches with the SCS modes.

The SCS modes are sensitive to $|\Delta c| = |\Delta u| = 1$ effects from BSM physics encoded in electromagnetic dipole couplings C_7 and C_7'. Branching ratios are in the $\sim 10^{-5} - 10^{-4}$ range, except for $D^+ \to K^+\bar{K}^0\gamma$ in QCDF, which is about one order of magnitude smaller due to smaller phase space, see Table. III. Not unexpected, we find that NP effects cannot be cleanly separated from the SM background in the branching ratio nor its distribution. On the other hand, $A_{\rm FB}$ allows for qualitatively different distributions, and to signal NP, see Fig. 6. The most clear-cut signals of NP are possible in CP-asymmetries, ideally in the Dalitz region, as in Fig. 8, but also in single differential distributions, see Fig. 9. The CP asymmetries can be sizable around resonance peaks, and reach $\mathcal{O}(0.1)$.

We conclude pointing out opportunities. The best decay channels for

- testing QCD frameworks: The CF mode $D^+ \to \pi^+\bar{K}^0\gamma$ because it has no leading order QCDF contribution. The same is true also the DCS mode $D_s \to K^+K^0\gamma$.

- testing the QCD frameworks with $A_{\rm FB}$, see Fig. 3: $D^0 \to \pi^0\overline{K}^0\gamma$ (CF), $D_s \to \pi^+\pi^0\gamma$ (CF) and $D^+ \to K^+\pi^0\gamma$ (DCS), which feature small uncertainties and a very distinctive shape which is reasonably well understood.

- testing the SM with $A_{\rm FB}$, see Fig. 6: $D^0 \to \pi^+\pi^-\gamma$, $D^+ \to \pi^+\pi^0\gamma$ and $D_s \to \pi^+K^0\gamma$ because differences between SM and BSM asymmetries in the other decays are small.

- testing the SM with $A_{\rm CP}$: Here one should distinguish between the single and double differential CP-asymmetries. Dalitz plots (Fig. 8) are suitable for all SCS decay channels. For $A_{\rm CP}(s)$

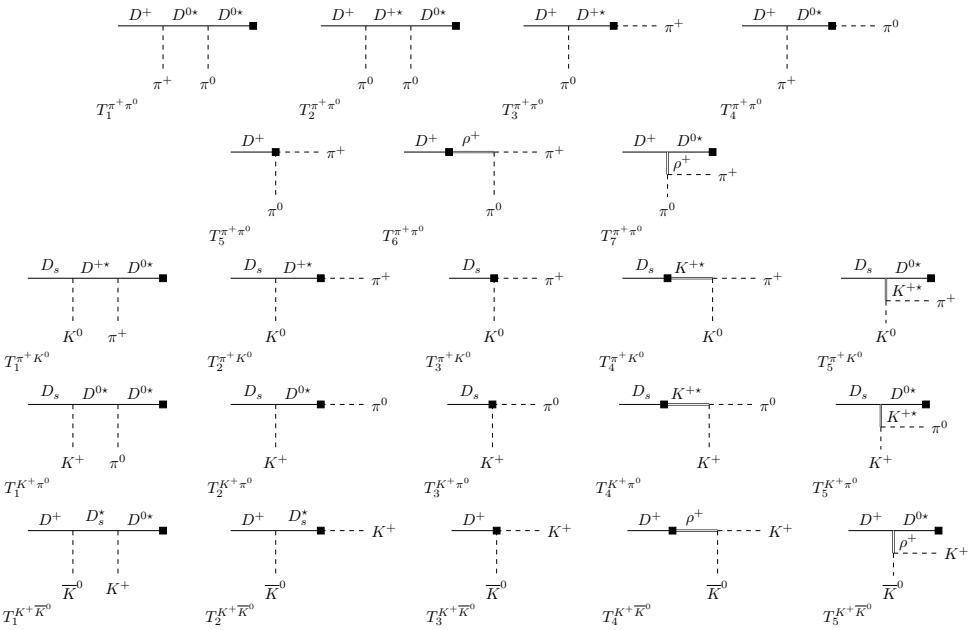

Figure 10: Feynman diagrams which contribute to the tensor form factors.

(Fig. 7, 9), the decays $D^+ \to \pi^+\pi^0\gamma$ and $D_s \to \pi^+ K^0\gamma$ can be emphasized, because they are sensitive to both BSM coefficients C_7 and C_7' and exhibit less cancellations between the t and u channel resonances. $D^0 \to K^+K^-\gamma$ is also a good option in the region of the Φ resonance. $D^0 \to \pi^+\pi^-\gamma$, $D^+ \to K^+\overline{K}^0\gamma$ and $D_s \to K^+\pi^0\gamma$ only have a good sensitivity in one of the BSM coefficients or smaller asymmetries have to be expected due to cancellations.

Appendix A: HHχPT form factors

The $D^+_{(s)} \to P^+P^0$ matrix elements of the tensor currents can be parameterized as

$$\langle P^+(p_1)P^0(p_2)|\overline{u}\sigma^{\mu\nu}k_\mu(1\pm\gamma_5)c|D^+_{(s)}(P)\rangle = m_D\left[a'p_1^\nu + b'p_2^\nu + c'P^\mu \mp 2ih'\epsilon^{\nu\alpha\beta\gamma}p_{1\alpha}p_{2\beta}k_\gamma\right]. \quad \text{(A1)}$$

The form factors a', b', c', h' depend on s and t and satisfy

$$a'p_1\cdot k + b'p_2\cdot k + c'P\cdot k = 0\,. \quad \text{(A2)}$$

The numerical values for the parameters in the form factors are given in appendix A of [10].

1. Cabibbo-favored decay modes

$\underline{D_s \to \pi^+\pi^0\gamma}$

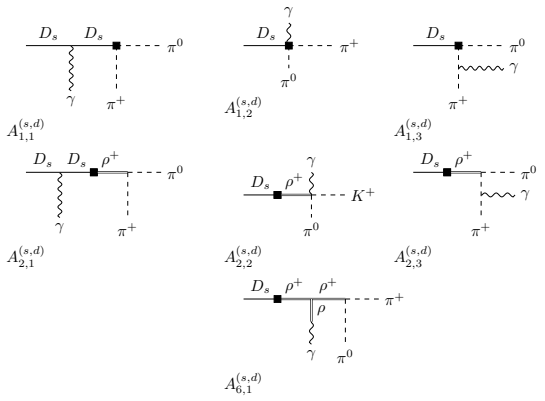

a) Contributions to the parity-even form factors A and E. Additionally, for each of the diagrams $A_{1,2}$, $A_{1,3}$ and $A_{2,3}$ there is another one where the photon is coupled via a vector meson.

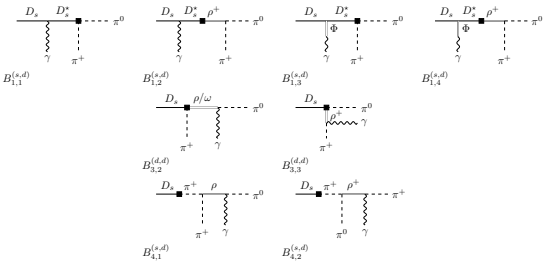

b) Contributions to the parity-odd form factors B and D.

Figure 11: Feynman diagrams contributing to the decay $D_s \to \pi^+\pi^0\gamma$ within the SM.

$$A_{1+2}^{(s,d)} = i\sqrt{2} f_{D_s} \frac{v\cdot p_2 - v\cdot p_1 - v\cdot k}{(v\cdot k)(p_1\cdot k)} \tag{A3}$$

$$A_{6}^{(s,d)} = i2\sqrt{2} f_{D_s} \frac{p_1\cdot p_2}{m_{D_s}(v\cdot k)} BW_{\rho^+}(p_1+p_2) \tag{A4}$$

$$B_{1}^{(s,d)} = \frac{f_{D_s}}{v\cdot k+\Delta}\left[1 - m_\rho^2 BW_{\rho^+}(p_1+p_2)\right]\left[2\sqrt{2}\lambda' - g_v\lambda\frac{2g_\Phi}{3m_\Phi^2}\right] \tag{A5}$$

$$B_{3}^{(s,d)} = -\frac{\sqrt{2} f_{D_s} g_\rho}{f_\pi}\left(g_{\rho\pi\gamma} BW_\rho(p_2+k) + g_{\rho^\pm\pi^\pm\gamma} BW_{\rho^+}(p_1+k)\right) \tag{A6}$$

$$B_{4}^{(s,d)} = \frac{\sqrt{2} m_{D_s}^2 f_{D_s} f_\pi m_\rho^2}{g_\rho(m_{D_s}^2 - m_\pi^2)}\left(g_{\rho\pi\gamma} BW_\rho(p_2+k) + g_{\rho^\pm\pi^\pm\gamma} BW_{\rho^+}(p_1+k)\right) \tag{A7}$$

$\underline{D_s \to K^+\overline{K}^0\gamma}$

$$A_{1+2}^{(s,d)} = -i f_{D_s} \frac{v\cdot p_2 - v\cdot p_1 - v\cdot k}{(v\cdot k)(p_1\cdot k)} \tag{A8}$$

$$A_{6}^{(s,d)} = -i2 f_{D_s} \frac{p_1\cdot p_2}{m_{D_s}(v\cdot k)} BW_{\rho^+}(p_1+p_2) \tag{A9}$$

$$E_{1}^{(s,d)} = -i f_{D_s} \frac{v\cdot p_2}{(v\cdot k)(p_1\cdot k)} \tag{A10}$$

$$E_{2}^{(s,d)} = -i\sqrt{\frac{m_D}{m_{D_s}}} f_D g \frac{p_1\cdot p_2 - (v\cdot p_1)(v\cdot p_2) + (v\cdot k)(m_{D_s} - v\cdot p_2)}{(v\cdot k + v\cdot p_1 + \Delta)(v\cdot k)(p_1\cdot k)} \tag{A11}$$

$$E_{3}^{(s,d)} = -i\sqrt{\frac{m_D}{m_{D_s}}} \frac{f_D g (v\cdot k)}{v\cdot k + v\cdot p_1 + \Delta}\left[\frac{2\lambda' + \frac{1}{\sqrt{2}} g_v\lambda\left(\frac{g_\omega}{3m_\omega^2} + \frac{g_\rho}{m_\rho^2}\right)}{v\cdot p_1 + \Delta} - \frac{2\lambda' - g_v\lambda\frac{\sqrt{2}g_\Phi}{3m_\Phi^2}}{v\cdot k + \Delta}\right] \tag{A12}$$

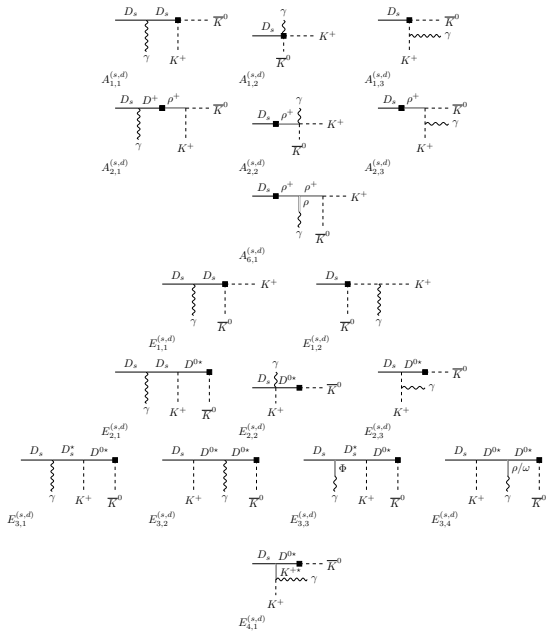

a) Contributions to the parity-even form factors A and E. Additionally, for each of the diagrams $A_{1,2}$, $A_{1,3}$, $A_{2,3}$, $E_{1,2}$ und $E_{2,3}$ there is another one where the photon is coupled via a vector meson.

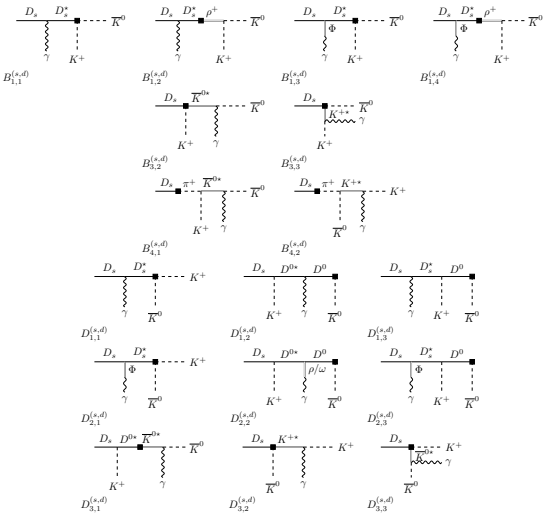

b) Contributions to the parity-odd form factors B and D.

Figure 12: Feynman diagrams contributing to the decay $D_s \to K^+\overline{K}^0\gamma$ within the SM.

$$B_1^{(s,d)} = -\frac{f_{D_s}}{v\cdot k+\Delta}\left[1-m_\rho^2 BW_{\rho^+}(p_1+p_2)\right]\left[2\lambda' - g_v\lambda\frac{\sqrt{2}g_\Phi}{3m_\Phi^2}\right] \tag{A13}$$

$$B_3^{(s,d)} = \frac{f_{D_s}g_{K^\star}}{f_K}\left(g_{K^\star K\gamma}BW_{K^\star}(p_2+k) + g_{K^{\pm\star}K^\pm\gamma}BW_{K^{+\star}}(p_1+k)\right) \tag{A14}$$

$$B_4^{(s,d)} = -\frac{m_{D_s}^2 f_{D_s} f_\pi}{m_{D_s}^2-m_\pi^2}\frac{m_{K^\star}^2}{g_{K^\star}}\left(g_{K^{\pm\star}K^\pm\gamma}BW_{K^{+\star}}(p_1+k) + g_{K^\star K\gamma}BW_{K^\star}(p_2+k)\right) \tag{A15}$$

$$D_1^{(s,d)} = -2\lambda'\left[\frac{f_{D_s}}{v\cdot k+\Delta} + \frac{\sqrt{m_D}f_D g(v\cdot p_2)}{\sqrt{m_{D_s}}(v\cdot k+v\cdot p_1)}\left(\frac{1}{v\cdot k+\Delta}+\frac{1}{v\cdot p_1+\Delta}\right)\right] \tag{A16}$$

$$D_2^{(s,d)} = -g_v\lambda\left[\frac{-f_{D_s}\frac{\sqrt{2}g_\Phi}{3m_\Phi^2}}{v\cdot k+\Delta} + \frac{\sqrt{m_D}f_D g(v\cdot p_2)}{\sqrt{m_{D_s}}(v\cdot k+v\cdot p_1)}\left(\frac{-\frac{\sqrt{2}g_\Phi}{3m_\Phi^2}}{v\cdot k+\Delta} + \frac{\frac{1}{\sqrt{2}}\left(\frac{g_\omega}{3m_\omega^2}+\frac{g_\rho}{m_\rho^2}\right)}{v\cdot p_1+\Delta}\right)\right] \tag{A17}$$

$$\begin{aligned} D_3^{(s,d)} = {} & \frac{g_{K^\star}g_{K^\star K\gamma}}{f_K}\left(f_{D_s}+\sqrt{\frac{m_D}{m_{D_s}}}f_D g\frac{m_{D_s}-v\cdot p_1}{v\cdot p_1+\Delta}\right)BW_{K^\star}(p_2+k) \\ & - \frac{2f_K\left(m_{D_s}\alpha_1-\alpha_2 v\cdot p_2\right)}{\sqrt{m_{D_s}}}\frac{m_{K^\star}^2}{g_{K^\star}}g_{K^{\pm\star}K^\pm\gamma}BW_{K^{+\star}}(p_1+k) \end{aligned} \tag{A18}$$

$\underline{D^+ \to \pi^+\overline{K}^0\gamma}$

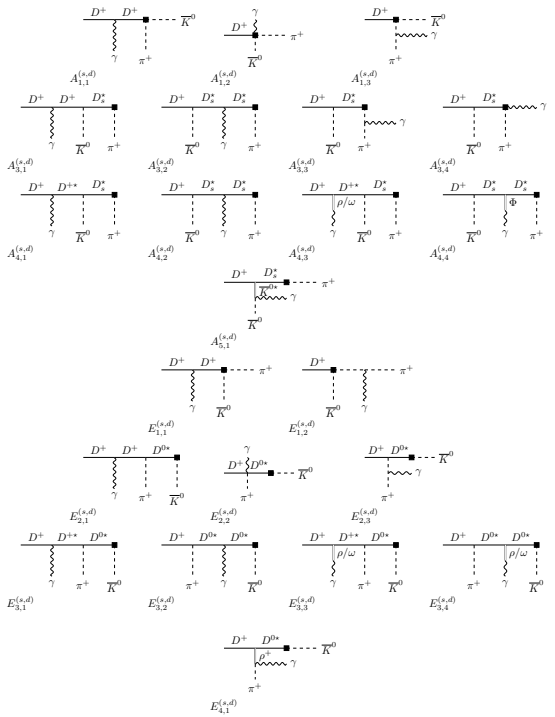

a) Contributions to the parity-even form factors A and E. For each of the diagrams $A_{1,2}$, $A_{1,3}$, $A_{3,3}$, $A_{3,4}$, $E_{1,2}$ und $E_{2,3}$ there is another one where the photon is coupled via a vector meson.

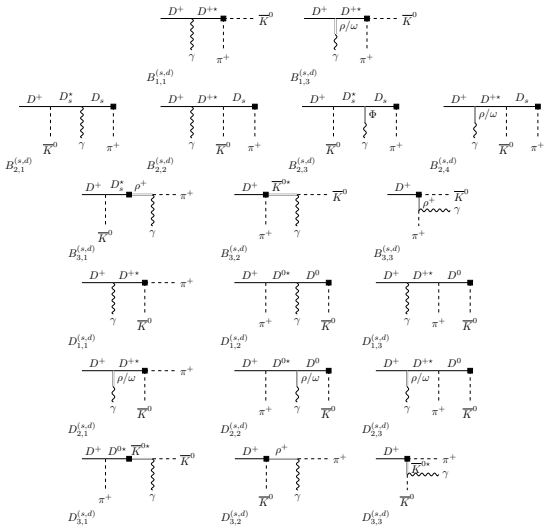

b) Contributions to the parity-odd form factors B and D.

Figure 13: Feynman diagrams contributing to the decay $D^+ \to \pi^+ \overline{K}^0 \gamma$ within the SM.

$$A_1^{(s,d)} = -i \frac{f_D f_\pi}{f_K} \frac{v \cdot p_1 + v \cdot k}{(v \cdot k)(p_1 \cdot k)} \tag{A19}$$

$$A_3^{(s,d)} = -i \sqrt{\frac{m_{D_s}}{m_D}} \frac{f_{D_s} f_\pi g}{f_K} \frac{p_1 \cdot p_2 - (v \cdot p_1)(v \cdot p_2) + (v \cdot k)(m_D - v \cdot p_2)}{(v \cdot p_2 + \Delta)(v \cdot k)(p_1 \cdot k)} \tag{A20}$$

$$A_4^{(s,d)} = -i \sqrt{\frac{m_{D_s}}{m_D}} \frac{f_{D_s} f_\pi g (v \cdot k)}{f_K (v \cdot k + v \cdot p_2 + \Delta)} \left[\frac{2\lambda' + \frac{1}{\sqrt{2}} g_v \lambda \left(\frac{g_\omega}{3 m_\omega^2} - \frac{g_\rho}{m_\rho^2} \right)}{v \cdot k + \Delta} - \frac{2\lambda' - \frac{\sqrt{2}}{3} g_v \lambda \frac{g_\Phi}{m_\Phi^2}}{v \cdot p_2 + \Delta} \right] \tag{A21}$$

$$E_1^{(s,d)} = -i \frac{f_D f_K}{f_\pi} \frac{v \cdot p_2}{(v \cdot k)(p_1 \cdot k)} \tag{A22}$$

$$E_2^{(s,d)} = -i \frac{f_D f_K g}{f_\pi} \frac{p_1 \cdot p_2 - (v \cdot p_1)(v \cdot p_2) + (v \cdot k)(m_D - v \cdot p_2)}{(v \cdot k + v \cdot p_1 + \Delta)(v \cdot k)(p_1 \cdot k)} \tag{A23}$$

$$E_3^{(s,d)} = -i \frac{f_D f_K g (v \cdot k)}{f_\pi (v \cdot k + v \cdot p_1 + \Delta)} \left[\frac{2\lambda' + \frac{1}{\sqrt{2}} g_v \lambda \left(\frac{g_\omega}{3 m_\omega^2} + \frac{g_\rho}{m_\rho^2} \right)}{v \cdot p_1 + \Delta} - \frac{2\lambda' + \frac{1}{\sqrt{2}} g_v \lambda \left(\frac{g_\omega}{3 m_\omega^2} - \frac{g_\rho}{m_\rho^2} \right)}{v \cdot k + \Delta} \right] \tag{A24}$$

$$B_1^{(s,d)} = \frac{f_D f_\pi}{f_K(v\cdot k+\Delta)}\left[2\lambda' + \frac{1}{\sqrt{2}} g_v \lambda \left(\frac{g_\omega}{3m_\omega^2} - \frac{g_\rho}{m_\rho^2}\right)\right] \tag{A25}$$

$$B_2^{(s,d)} = \sqrt{\frac{m_{D_s}}{m_D}}\frac{f_{D_s} f_\pi g(v\cdot p_1)}{f_K(v\cdot k + v\cdot p_2)}\left[\frac{2\lambda' - \frac{\sqrt{2}}{3} g_v\lambda \frac{g_\Phi}{m_\Phi^2}}{v\cdot p_2+\Delta} + \frac{2\lambda' + \frac{1}{\sqrt{2}} g_v\lambda\left(\frac{g_\omega}{3m_\omega^2} - \frac{g_\rho}{m_\rho^2}\right)}{v\cdot k+\Delta}\right] \tag{A26}$$

$$\begin{aligned} B_3^{(s,d)} = & -\frac{g_\rho g_{\rho^\pm\pi^\pm\gamma}}{f_K}\left(f_D + \sqrt{\frac{m_{D_s}}{m_D}} f_{D_s} g \frac{m_D - v\cdot p_2}{v\cdot p_2+\Delta}\right) BW_{\rho^+}(p_1+k) \\ & + \frac{2 f_\pi (m_D\alpha_1 - \alpha_2 v\cdot p_1)}{\sqrt{m_D}} \frac{m_{K^\star}^2}{g_{K^\star}} g_{K^\star K\gamma} BW_{K^\star}(p_2+k) \end{aligned} \tag{A27}$$

$$D_1^{(s,d)} = -2\frac{f_D f_K}{f_\pi}\lambda'\left[\frac{1}{v\cdot k+\Delta} + \frac{g(v\cdot p_2)}{v\cdot k + v\cdot p_1}\left(\frac{1}{v\cdot k+\Delta} + \frac{1}{v\cdot p_1+\Delta}\right)\right] \tag{A28}$$

$$D_2^{(s,d)} = -\frac{f_D f_K g_v \lambda}{\sqrt{2} f_\pi}\left[\frac{\frac{g_\omega}{3m_\omega^2} - \frac{g_\rho}{m_\rho^2}}{v\cdot k+\Delta} + \frac{g(v\cdot p_2)}{v\cdot k + v\cdot p_1}\left(\frac{\frac{g_\omega}{3m_\omega^2} - \frac{g_\rho}{m_\rho^2}}{v\cdot k+\Delta} + \frac{\frac{g_\omega}{3m_\omega^2} + \frac{g_\rho}{m_\rho^2}}{v\cdot p_1+\Delta}\right)\right] \tag{A29}$$

$$\begin{aligned} D_3^{(s,d)} = & \frac{f_D g_{K^\star} g_{K^\star K\gamma}}{f_\pi}\left(1 + g\frac{m_D - v\cdot p_1}{v\cdot p_1+\Delta}\right) BW_{K^\star}(p_2+k) \\ & - \frac{2 f_K\,(m_D\alpha_1 - \alpha_2 v\cdot p_2)}{\sqrt{m_D}} \frac{m_\rho^2}{g_\rho} g_{\rho^\pm\pi^\pm\gamma} BW_{\rho^+}(p_1+k) \end{aligned} \tag{A30}$$

2. Singly Cabibbo-suppressed decay modes

$\underline{D^+ \to \pi^+\pi^0\gamma}$

$$A_{1+2}^{(d,d)} = i\sqrt{2} f_D \frac{v\cdot p_2 - v\cdot p_1 - v\cdot k}{(v\cdot k)(p_1\cdot k)} + i\frac{f_D}{\sqrt{2}}\frac{v\cdot p_1 + v\cdot k}{(v\cdot k)(p_1\cdot k)} \tag{A31}$$

$$A_3^{(d,d)} = i\frac{f_D g}{\sqrt{2}}\frac{p_1\cdot p_2 - (v\cdot p_1)(v\cdot p_2) + (v\cdot k)(m_D - v\cdot p_2)}{(v\cdot p_2+\Delta)(v\cdot k)(p_1\cdot k)} \tag{A32}$$

$$A_4^{(d,d)} = i\frac{f_D g(v\cdot k)}{v\cdot k + v\cdot p_2 + \Delta}\left[\frac{\sqrt{2}\lambda' + \frac{1}{2} g_v\lambda\left(\frac{g_\omega}{3m_\omega^2} - \frac{g_\rho}{m_\rho^2}\right)}{v\cdot k+\Delta} - \frac{\sqrt{2}\lambda' + \frac{1}{2} g_v\lambda\left(\frac{g_\omega}{3m_\omega^2} - \frac{g_\rho}{m_\rho^2}\right)}{v\cdot p_2+\Delta}\right] \tag{A33}$$

$$A_6^{(d,d)} = i2\sqrt{2} f_D \frac{p_1\cdot p_2}{m_D(v\cdot k)} BW_{\rho^+}(p_1+p_2) \tag{A34}$$

$$E_1^{(d,d)} = i\frac{f_D}{\sqrt{2}}\frac{v\cdot p_2}{(v\cdot k)(p_1\cdot k)} \tag{A35}$$

$$E_2^{(d,d)} = i\frac{f_D g}{\sqrt{2}}\frac{p_1\cdot p_2 - (v\cdot p_1)(v\cdot p_2) + (v\cdot k)(m_D - v\cdot p_2)}{(v\cdot k + v\cdot p_1+\Delta)(v\cdot k)(p_1\cdot k)} \tag{A36}$$

$$E_3^{(d,d)} = i\frac{f_D g(v\cdot k)}{v\cdot k + v\cdot p_1 + \Delta}\left[\frac{\sqrt{2}\lambda' + \frac{1}{2} g_v\lambda\left(\frac{g_\omega}{3m_\omega^2} + \frac{g_\rho}{m_\rho^2}\right)}{v\cdot p_1+\Delta} - \frac{\sqrt{2}\lambda' + \frac{1}{2} g_v\lambda\left(\frac{g_\omega}{3m_\omega^2} - \frac{g_\rho}{m_\rho^2}\right)}{v\cdot k+\Delta}\right] \tag{A37}$$

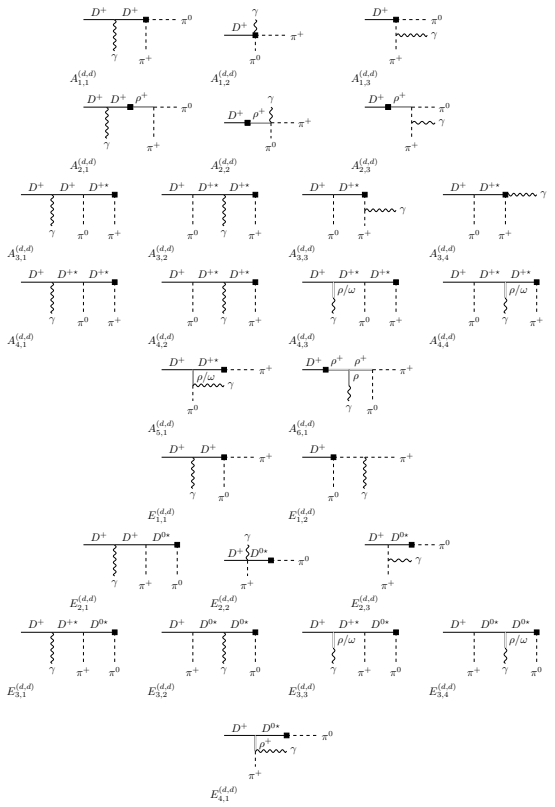

a) Contributions to the parity-even form factors A and E. Note that the diagrams A_1 have two different factorizations. Additionally, for each of the diagrams $A_{1,2}$, $A_{1,3}$, $A_{2,3}$, $A_{3,3}$, $A_{3,4}$, $E_{1,2}$ und $E_{2,3}$ there is another one where the photon is coupled via a vector meson.

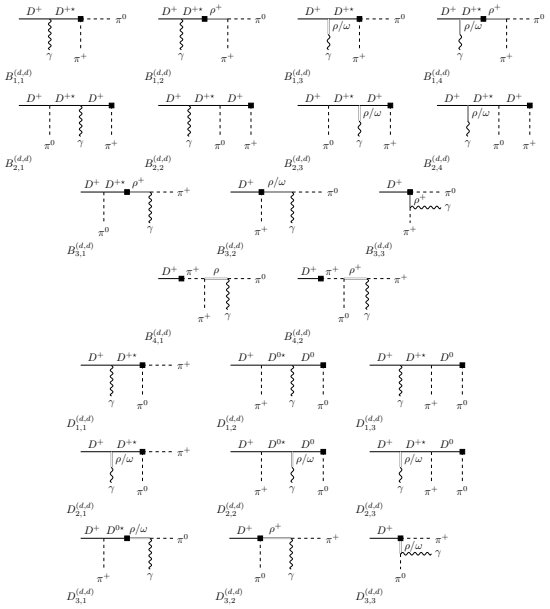

b) Contributions to the parity-odd form factors B and D. Note that the diagrams $B_{1,1/3}$ and $B_{3,2/3}$ have two different factorizations.

Figure 14: Feynman diagrams contributing to the decay $D^+ \to \pi^+\pi^0\gamma$ within the SM.

$$B_1^{(d,d)} = \frac{f_D}{v\cdot k+\Delta}\left[\frac{1}{2} - m_\rho^2 BW_{\rho^+}(p_1+p_2)\right]\left[2\sqrt{2}\lambda' + g_v\lambda\left(\frac{g_\omega}{3m_\omega^2} - \frac{g_\rho}{m_\rho^2}\right)\right] \tag{A38}$$

$$B_2^{(d,d)} = -\frac{f_D g(v\cdot p_1)}{v\cdot k + v\cdot p_2}\left[\frac{\sqrt{2}\lambda' + \frac{1}{2}g_v\lambda\left(\frac{g_\omega}{3m_\omega^2} - \frac{g_\rho}{m_\rho^2}\right)}{v\cdot p_2+\Delta} + \frac{\sqrt{2}\lambda' + \frac{1}{2}g_v\lambda\left(\frac{g_\omega}{3m_\omega^2} - \frac{g_\rho}{m_\rho^2}\right)}{v\cdot k+\Delta}\right] \tag{A39}$$

$$\begin{aligned} B_3^{(d,d)} &= \frac{f_D g_\rho g_{\rho^\pm\pi^\pm\gamma}}{\sqrt{2}f_\pi}\left(1 + g\frac{m_D - v\cdot p_2}{v\cdot p_2+\Delta}\right)BW_{\rho^+}(p_1+k) \\ &+ \frac{\sqrt{2}f_\pi(m_D\alpha_1 - \alpha_2 v\cdot p_1)}{\sqrt{m_D}}\left(\frac{m_\omega^2}{g_\omega}g_{\omega\pi\gamma}BW_\omega(p_2+k) - \frac{m_\rho^2}{g_\rho}g_{\rho\pi\gamma}BW_\rho(p_2+k)\right) \\ &- \frac{\sqrt{2}f_D g_\rho}{f_\pi}\left(g_{\rho\pi\gamma}BW_\rho(p_2+k) + g_{\rho^\pm\pi^\pm\gamma}BW_{\rho^+}(p_1+k)\right) \end{aligned} \tag{A40}$$

$$B_4^{(d,d)} = \frac{\sqrt{2}m_D^2 f_D f_\pi m_\rho^2}{g_\rho(m_D^2 - m_\pi^2)}\left(g_{\rho\pi\gamma}BW_\rho(p_2+k) + g_{\rho^\pm\pi^\pm\gamma}BW_{\rho^+}(p_1+k)\right) \tag{A41}$$

$$D_1^{(d,d)} = \sqrt{2}f_D\lambda'\left[\frac{1}{v\cdot k+\Delta} + \frac{g(v\cdot p_2)}{v\cdot k + v\cdot p_1}\left(\frac{1}{v\cdot k+\Delta} + \frac{1}{v\cdot p_1+\Delta}\right)\right] \tag{A42}$$

$$D_2^{(d,d)} = \frac{f_D g_v\lambda}{2}\left[\frac{\frac{g_\omega}{3m_\omega^2} - \frac{g_\rho}{m_\rho^2}}{v\cdot k+\Delta} + \frac{g(v\cdot p_2)}{v\cdot k + v\cdot p_1}\left(\frac{\frac{g_\omega}{3m_\omega^2} - \frac{g_\rho}{m_\rho^2}}{v\cdot k+\Delta} + \frac{\frac{g_\omega}{3m_\omega^2} + \frac{g_\rho}{m_\rho^2}}{v\cdot p_1+\Delta}\right)\right] \tag{A43}$$

$$\begin{aligned} D_3^{(d,d)} &= \frac{f_D}{\sqrt{2}f_\pi}\left(1 + g\frac{m_D - v\cdot p_1}{v\cdot p_1+\Delta}\right)\left(g_\omega g_{\omega\pi\gamma}BW_\omega(p_2+k) - g_\rho g_{\rho\pi\gamma}BW_\rho(p_2+k)\right) \\ &+ \frac{\sqrt{2}f_\pi\left(m_D\alpha_1 - \alpha_2 v\cdot p_2\right)}{\sqrt{m_D}}\frac{m_\rho^2}{g_\rho}g_{\rho^\pm\pi^\pm\gamma}BW_{\rho^+}(p_1+k) \end{aligned} \tag{A44}$$

$$\begin{aligned} a' &= \frac{f_D g(v\cdot k)}{\sqrt{2}f_\pi^2(v\cdot p_1+\Delta)} + \frac{f_D g^2\left(p_2\cdot k - (v\cdot k)(v\cdot p_2)\right)}{\sqrt{2}f_\pi^2(v\cdot p_1 + v\cdot p_2+\Delta)}\left[\frac{1}{v\cdot p_1+\Delta} + \frac{1}{v\cdot p_2+\Delta}\right] \\ &- \frac{\sqrt{2}\alpha_1(v\cdot k)}{f_\pi^2\sqrt{m_D}}\left(1 + \frac{f_\pi^2 m_\rho^4}{g_\rho^2}BW_{\rho^+}(p_1+p_2)\right) \\ &+ \frac{2f_D\lambda g_v m_\rho^2\left(p_2\cdot k - (v\cdot k)(v\cdot p_2)\right)}{g_\rho(v\cdot p_1 + v\cdot p_2+\Delta)}BW_{\rho^+}(p_1+p_2) \end{aligned} \tag{A45}$$

$$\begin{aligned} b' &= -\frac{f_D g(v\cdot k)}{\sqrt{2}f_\pi^2(v\cdot p_2+\Delta)} - \frac{f_D g^2\left(p_1\cdot k - (v\cdot k)(v\cdot p_1)\right)}{\sqrt{2}f_\pi^2(v\cdot p_1 + v\cdot p_2+\Delta)}\left[\frac{1}{v\cdot p_1+\Delta} + \frac{1}{v\cdot p_2+\Delta}\right] \\ &+ \frac{\sqrt{2}\alpha_1(v\cdot k)}{f_\pi^2\sqrt{m_D}}\left(1 + \frac{f_\pi^2 m_\rho^4}{g_\rho^2}BW_{\rho^+}(p_1+p_2)\right) \\ &- \frac{2f_D\lambda g_v m_\rho^2\left(p_1\cdot k - (v\cdot k)(v\cdot p_1)\right)}{g_\rho(v\cdot p_1 + v\cdot p_2+\Delta)}BW_{\rho^+}(p_1+p_2) \end{aligned} \tag{A46}$$

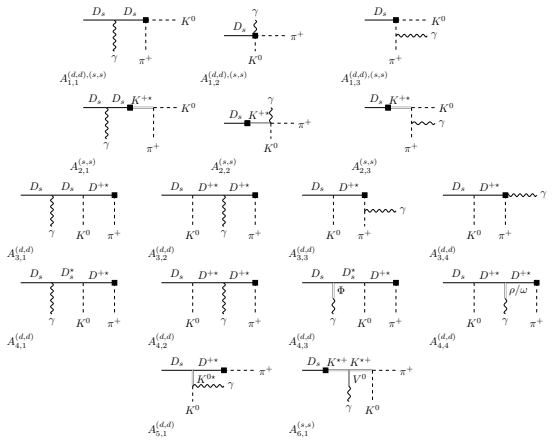

a) Contributions to the parity-even form factors A and E. Note that the diagrams A_1 have two different factorizations. Additionally, for each of the diagrams $A_{1,2}$, $A_{1,3}$, $A_{2,3}$, $A_{3,3}$ and $A_{3,4}$ there is another one where the photon is coupled via a vector meson.

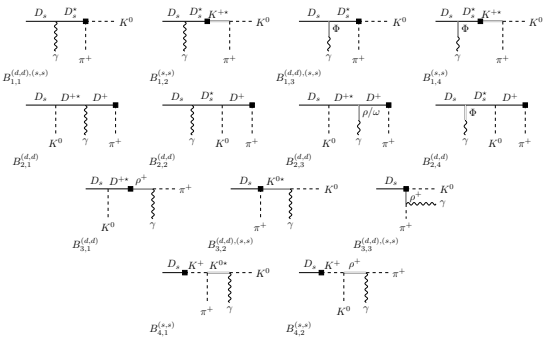

b) Contributions to the parity-odd form factors B and D. Note that the diagrams $B_{1,1/3}$ and $B_{3,2/3}$ have two different factorizations.

Figure 15: Feynman diagrams contributing to the decay $D_s \to \pi^+ K^0 \gamma$ within the SM.

$$
\begin{aligned}
c' = & \frac{f_D g}{\sqrt{2} m_D f_\pi^2} \left(\frac{p_2 \cdot k}{v \cdot p_2 + \Delta} - \frac{p_1 \cdot k}{v \cdot p_1 + \Delta} \right) \\
& - \frac{f_D g^2 \left((p_2 \cdot k)(v \cdot p_1) - (p_1 \cdot k)(v \cdot p_2) \right)}{\sqrt{2} m_D f_\pi^2 (v \cdot p_1 + v \cdot p_2 + \Delta)} \left(\frac{1}{v \cdot p_1 + \Delta} + \frac{1}{v \cdot p_2 + \Delta} \right) \\
& + \frac{\sqrt{2} \alpha_1 (p_1 \cdot k - p_2 \cdot k)}{\sqrt{m_D^3 f_\pi^2}} \left(1 + \frac{f_\pi^2 m_\rho^4}{g_\rho^2} BW_{\rho^+}(p_1 + p_2) \right) \\
& - \frac{2 f_D \lambda g_v m_\rho^2 \left((p_2 \cdot k)(v \cdot p_1) - (p_1 \cdot k)(v \cdot p_2) \right)}{g_\rho m_D (v \cdot p_1 + v \cdot p_2 + \Delta)} BW_{\rho^+}(p_1 + p_2)
\end{aligned}
\tag{A47}
$$

$$
\begin{aligned}
h' = & - \frac{f_D g}{2\sqrt{2} m_D f_\pi^2} \left(\frac{1}{v \cdot p_1 + \Delta} + \frac{1}{v \cdot p_2 + \Delta} \right) \left(1 + g \frac{v \cdot k}{v \cdot p_1 + v \cdot p_2 + \Delta} \right) \\
& - \frac{\sqrt{2} \alpha_1}{\sqrt{m_D^3 f_\pi^2}} \left(1 + \frac{f_\pi^2 m_\rho^4}{g_\rho^2} BW_{\rho^+}(p_1 + p_2) \right) \\
& - \frac{f_D \lambda g_v m_\rho^2 (v \cdot k)}{g_\rho m_D (v \cdot p_1 + v \cdot p_2 + \Delta)} BW_{\rho^+}(p_1 + p_2)
\end{aligned}
\tag{A48}
$$

$\underline{D_s \to \pi^+ K^0 \gamma}$

$$A_1^{(d,d)} = -i\frac{f_{D_s}f_\pi}{f_K}\frac{v\cdot p_1 + v\cdot k}{(v\cdot k)(p_1\cdot k)}$$
$$A_{1+2}^{(s,s)} = -if_{D_s}\frac{v\cdot p_2 - v\cdot p_1 - v\cdot k}{(v\cdot k)(p_1\cdot k)} \tag{A49}$$

$$A_3^{(d,d)} = -i\frac{f_{D_s}f_\pi g}{f_K}\frac{p_1\cdot p_2 - (v\cdot p_1)(v\cdot p_2) + (v\cdot k)(M - v\cdot p_2)}{(v\cdot p_2+\Delta)(v\cdot k)(p_1\cdot k)} \tag{A50}$$

$$A_4^{(d,d)} = -i\frac{\sqrt{m_D}f_D f_\pi g(v\cdot k)}{\sqrt{m_{D_s}}f_K(v\cdot k + v\cdot p_2 + \Delta)}\left[\frac{2\lambda' - \frac{\sqrt{2}}{3}g_v\lambda\frac{g_\Phi}{m_\Phi^2}}{v\cdot k+\Delta} - \frac{2\lambda' + \frac{1}{\sqrt{2}}g_v\lambda\left(\frac{g_\omega}{3m_\omega^2} - \frac{g_\rho}{m_\rho^2}\right)}{v\cdot p_2+\Delta}\right] \tag{A51}$$

$$A_6^{(s,s)} = -i2f_{D_s}\frac{p_1\cdot p_2}{m_{D_s}(v\cdot k)}BW_{K^{\star+}}(p_1+p_2) \tag{A52}$$

$$B_1^{(d,d)} = \frac{f_{D_s}f_\pi}{f_K(v\cdot k+\Delta)}\left[2\lambda' - \frac{\sqrt{2}}{3}g_v\lambda\frac{g_\Phi}{m_\Phi^2}\right]$$
$$B_1^{(s,s)} = -\frac{f_{D_s}}{v\cdot k+\Delta}\left[1 - m_{K^\star}^2 BW_{K^{+\star}}(p_1+p_2)\right]\left[2\lambda' - \frac{\sqrt{2}}{3}g_v\lambda\frac{g_\Phi}{m_\Phi}\right] \tag{A53}$$

$$B_2^{(d,d)} = \frac{\sqrt{m_D}f_D f_\pi g(v\cdot p_1)}{\sqrt{m_{D_s}}f_K(v\cdot k + v\cdot p_2)}\left[\frac{2\lambda' + \frac{1}{\sqrt{2}}g_v\lambda\left(\frac{g_\omega}{3m_\omega^2} - \frac{g_\rho}{m_\rho^2}\right)}{v\cdot p_2+\Delta} + \frac{2\lambda' - \frac{\sqrt{2}}{3}g_v\lambda\frac{g_\Phi}{m_\Phi^2}}{v\cdot k+\Delta}\right] \tag{A54}$$

$$B_3^{(d,d)} = -\frac{g_\rho g_{\rho^\pm\pi^\pm\gamma}}{f_K}\left(f_{D_s} + gf_D\sqrt{\frac{m_D}{m_{D_s}}}\frac{m_{D_s} - v\cdot p_2}{v\cdot p_2+\Delta}\right)BW_{\rho^+}(p_1+k)$$
$$+ \frac{2f_\pi(m_{D_s}\alpha_1 - \alpha_2 v\cdot p_1)}{\sqrt{m_{D_s}}}\frac{m_{K^\star}^2}{g_{K^\star}}g_{K^\star K\gamma}BW_{K^\star}(p_2+k)) \tag{A55}$$

$$B_3^{(s,s)} = \frac{f_{D_s}g_{K^\star}}{f_\pi}g_{K^\star K\gamma}BW_{K^\star}(p_2+k) + \frac{f_{D_s}g_\rho}{f_K}g_{\rho^\pm\pi^\pm\gamma}BW_{\rho^+}(p_1+k)$$

$$B_4^{(s,s)} = -\frac{m_{D_s}^2 f_{D_s}f_K}{(m_{D_s}^2 - m_K^2)}\left(\frac{m_{K^\star}^2}{g_{K^\star}}g_{K^\star K\gamma}BW_{K^\star}(p_2+k) + \frac{m_\rho^2}{g_\rho}g_{\rho^\pm\pi^\pm\gamma}BW_{\rho^+}(p_1+k)\right) \tag{A56}$$

$$a' = -\frac{\sqrt{m_D}f_D g^2\left(p_2\cdot k - (v\cdot k)(v\cdot p_2)\right)}{f_\pi f_K\sqrt{m_{D_s}}(v\cdot p_1 + v\cdot p_2 + \Delta)(v\cdot p_2+\Delta)}$$
$$+ \frac{\alpha_1(v\cdot k)}{f_\pi f_K\sqrt{m_{D_s}}}\left(1 + \frac{f_\pi f_K m_{K^\star}^4}{g_{K^\star}^2}BW_{K^{+\star}}(p_1+p_2)\right)$$
$$- \frac{\sqrt{2m_D}f_D\lambda g_v m_{K^\star}^2\left(p_2\cdot k - (v\cdot k)(v\cdot p_2)\right)}{g_{K^\star}\sqrt{m_{D_s}}(v\cdot p_1 + v\cdot p_2 + \Delta)}BW_{K^{+\star}}(p_1+p_2) \tag{A57}$$

$$b' = \frac{\sqrt{m_D}f_D g}{f_\pi f_K\sqrt{m_{D_s}}(v\cdot p_2+\Delta)}\left[v\cdot k + g\frac{p_1\cdot k - (v\cdot k)(v\cdot p_1)}{v\cdot p_1 + v\cdot p_2 + \Delta}\right]$$
$$- \frac{\alpha_1(v\cdot k)}{f_\pi f_K\sqrt{m_{D_s}}}\left(1 + \frac{f_\pi f_K m_{K^\star}^4}{g_{K^\star}^2}BW_{K^{+\star}}(p_1+p_2)\right)$$
$$+ \frac{\sqrt{2m_D}f_D\lambda g_v m_{K^\star}^2\left(p_1\cdot k - (v\cdot k)(v\cdot p_1)\right)}{g_{K^\star}\sqrt{m_{D_s}}(v\cdot p_1 + v\cdot p_2 + \Delta)}BW_{K^{+\star}}(p_1+p_2) \tag{A58}$$

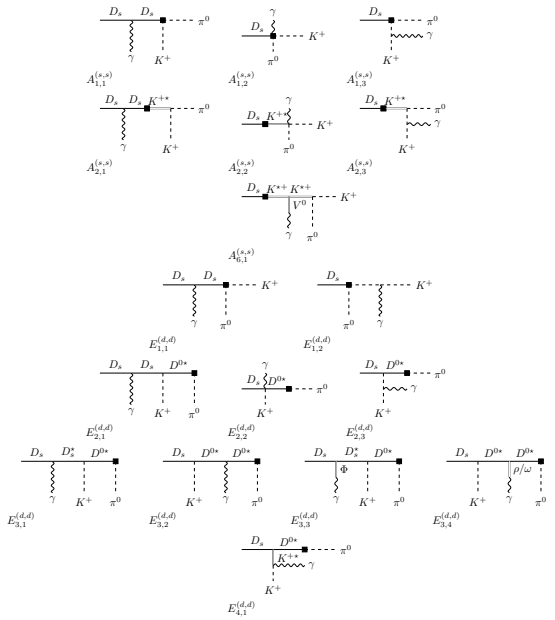

a) Contributions to the parity-even form factors A and E. Additionally, for each of the diagrams $A_{1,2}$, $A_{1,3}$, $A_{2,3}$, $E_{1,2}$ und $E_{2,3}$ there is another one where the photon is coupled via a vector meson.

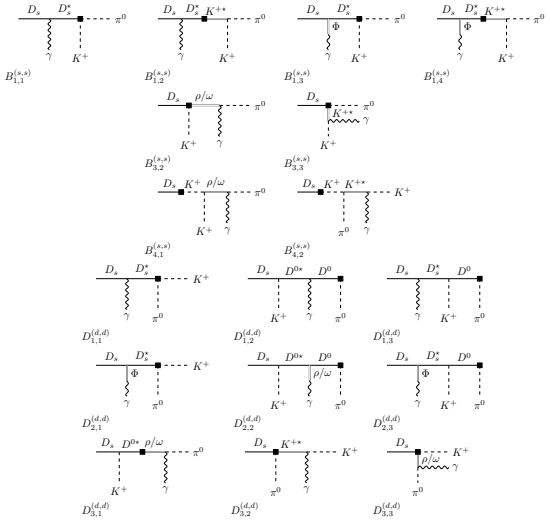

b) Contributions to the parity-odd form factors B and D.

Figure 16: Feynman diagrams contributing to the decay $D_s \to K^+\pi^0\gamma$ within the SM.

$$
\begin{aligned}
c' = &-\frac{\sqrt{m_D} f_D g}{\sqrt{m_{D_s}^3} f_\pi f_K (v\cdot p_2 + \Delta)} \left[p_2 \cdot k - g \frac{(p_2\cdot k)(v\cdot p_1) - (p_1\cdot k)(v\cdot p_2)}{v\cdot p_1 + v\cdot p_2 + \Delta} \right] \\
&- \frac{\alpha_1 (p_1\cdot k - p_2\cdot k)}{\sqrt{m_{D_s}^3} f_\pi f_K} \left(1 + \frac{f_\pi f_K m_{K^\star}^4}{g_{K^\star}^2} BW_{K^{+\star}}(p_1+p_2) \right) \\
&+ \frac{\sqrt{2m_D} f_D \lambda g_v m_{K^\star}^2 \left((p_2\cdot k)(v\cdot p_1) - (p_1\cdot k)(v\cdot p_2) \right)}{\sqrt{m_{D_s}^3} g_{K^\star} (v\cdot p_1 + v\cdot p_2 + \Delta)} BW_{K^{+\star}}(p_1+p_2)
\end{aligned}
\tag{A59}
$$

$$
\begin{aligned}
h' = &\frac{\sqrt{m_D} f_D g}{2\sqrt{m_{D_s}^3} f_\pi f_K (v\cdot p_2 + \Delta)} \left(1 + g \frac{v\cdot k}{v\cdot p_1 + v\cdot p_2 + \Delta} \right) \\
&+ \frac{\alpha_1}{\sqrt{m_{D_s}^3} f_\pi f_K} \left(1 + \frac{f_\pi f_K m_{K^\star}^4}{g_{K^\star}^2} BW_{K^{+\star}}(p_1+p_2) \right) \\
&+ \frac{\sqrt{m_D} f_D \lambda g_v m_{K^\star}^2 (v\cdot k)}{\sqrt{2m_{D_s}^3} g_{K^\star} (v\cdot p_1 + v\cdot p_2 + \Delta)} BW_{K^{+\star}}(p_1+p_2)
\end{aligned}
\tag{A60}
$$

$\underline{D_s \to K^+\pi^0\gamma}$

$$A_{1+2}^{(s,s)} = i\frac{f_{D_s}}{\sqrt{2}}\frac{v\cdot p_2 - v\cdot p_1 - v\cdot k}{(v\cdot k)(p_1\cdot k)} \tag{A61}$$

$$A_{6}^{(s,s)} = i\sqrt{2}f_{D_s}\frac{p_1\cdot p_2}{m_{D_s}(v\cdot k)}BW_{K^{\star+}}(p_1+p_2) \tag{A62}$$

$$E_1^{(d,d)} = i\frac{f_{D_s}f_\pi}{\sqrt{2}f_K}\frac{v\cdot p_2}{(v\cdot k)(p_1\cdot k)} \tag{A63}$$

$$E_2^{(d,d)} = i\sqrt{\frac{m_D}{m_{D_s}}}\frac{f_D f_\pi g}{\sqrt{2}f_K}\frac{p_1\cdot p_2 - (v\cdot p_1)(v\cdot p_2) + (v\cdot k)(m_{D_s} - v\cdot p_2)}{(v\cdot k + v\cdot p_1 + \Delta)(v\cdot k)(p_1\cdot k)} \tag{A64}$$

$$E_3^{(d,d)} = i\sqrt{\frac{m_D}{m_{D_s}}}\frac{f_D f_\pi g(v\cdot k)}{f_K(v\cdot k + v\cdot p_1 + \Delta)}\left[\frac{\sqrt{2}\lambda' + \frac{1}{2}g_v\lambda\left(\frac{g_\omega}{3m_\omega^2} + \frac{g_\rho}{m_\rho^2}\right)}{v\cdot p_1 + \Delta} - \frac{\sqrt{2}\lambda' - g_v\lambda\frac{g_\Phi}{3m_\Phi^2}}{v\cdot k + \Delta}\right] \tag{A65}$$

$$B_1^{(s,s)} = \frac{f_{D_s}}{v\cdot k + \Delta}\left[1 - m_{K^\star}^2 BW_{K^{+\star}}(p_1+p_2)\right]\left[\sqrt{2}\lambda' - g_v\lambda\frac{g_\Phi}{3m_\Phi^2}\right] \tag{A66}$$

$$B_3^{(s,s)} = -\frac{f_{D_s}g_\rho}{\sqrt{2}f_K}g_{\rho\pi\gamma}BW_\rho(p_2+k) - \frac{f_{D_s}g_\omega}{\sqrt{2}f_K}g_{\omega\pi\gamma}BW_\omega(p_2+k) - \frac{f_{D_s}g_{K^\star}}{\sqrt{2}f_\pi}g_{K^{\pm\star}K^\pm\gamma}BW_{K^{+\star}}(p_1+k) \tag{A67}$$

$$B_4^{(s,s)} = \frac{m_{D_s}^2 f_{D_s} f_K}{\sqrt{2}(m_{D_s}^2 - m_K^2)}\left(\frac{2m_{K^\star}^2}{g_{K^\star}}g_{K^{\pm\star}K^\pm\gamma}BW_{K^{+\star}}(p_1+k) + \frac{m_\rho^2}{g_\rho}g_{\rho\pi\gamma}BW_\rho(p_2+k) + \frac{m_\omega^2}{g_\omega}g_{\omega\pi\gamma}BW_\omega(p_2+k)\right) \tag{A68}$$

$$D_1^{(d,d)} = \sqrt{2}\frac{f_\pi}{f_K}\lambda'\left[\frac{f_{D_s}}{v\cdot k + \Delta} + \frac{\sqrt{m_D}f_D g(v\cdot p_2)}{\sqrt{m_{D_s}}(v\cdot k + v\cdot p_1)}\left(\frac{1}{v\cdot k + \Delta} + \frac{1}{v\cdot p_1 + \Delta}\right)\right] \tag{A69}$$

$$D_2^{(d,d)} = \frac{f_\pi g_v\lambda}{f_K}\left[\frac{-f_{D_s}\frac{g_\Phi}{3m_\Phi^2}}{v\cdot k + \Delta} + \frac{\sqrt{m_D}f_D g(v\cdot p_2)}{\sqrt{m_{D_s}}(v\cdot k + v\cdot p_1)}\left(\frac{-\frac{g_\Phi}{3m_\Phi^2}}{v\cdot k + \Delta} + \frac{\frac{1}{2}\left(\frac{g_\omega}{3m_\omega^2} + \frac{g_\rho}{m_\rho^2}\right)}{v\cdot p_1 + \Delta}\right)\right] \tag{A70}$$

$$\begin{aligned} D_3^{(d,d)} = {} & \frac{1}{\sqrt{2}f_K}\left(f_{D_s} + \sqrt{\frac{m_D}{m_{D_s}}}f_D g\frac{m_{D_s} - v\cdot p_1}{v\cdot p_1 + \Delta}\right)\left(g_\omega g_{\omega\pi\gamma}BW_\omega(p_2+k) - g_\rho g_{\rho\pi\gamma}BW_\rho(p_2+k)\right) \\ & + \frac{\sqrt{2}f_\pi\left(m_{D_s}\alpha_1 - \alpha_2 v\cdot p_2\right)}{\sqrt{m_{D_s}}}\frac{m_{K^\star}^2}{g_{K^\star}}g_{K^{\pm\star}K^\pm\gamma}BW_{K^{+\star}}(p_1+k) \end{aligned} \tag{A71}$$

$$\begin{aligned} a' = {} & \frac{\sqrt{m_D}f_D g}{\sqrt{2}f_\pi f_K\sqrt{m_{D_s}}(v\cdot p_1 + \Delta)}\left[v\cdot k + g\frac{p_2\cdot k - (v\cdot k)(v\cdot p_2)}{v\cdot p_1 + v\cdot p_2 + \Delta}\right] \\ & - \frac{\alpha_1(v\cdot k)}{\sqrt{2}f_\pi f_K\sqrt{m_{D_s}}}\left(1 + \frac{f_\pi f_K m_{K^\star}^4}{g_{K^\star}^2}BW_{K^{+\star}}(p_1+p_2)\right) \\ & + \frac{\sqrt{m_D}f_D\lambda g_v m_{K^\star}^2\left(p_2\cdot k - (v\cdot k)(v\cdot p_2)\right)}{g_{K^\star}\sqrt{m_{D_s}}(v\cdot p_1 + v\cdot p_2 + \Delta)}BW_{K^{+\star}}(p_1+p_2) \end{aligned} \tag{A72}$$

$$
\begin{aligned}
b' = & -\frac{\sqrt{m_D} f_D g^2 \left(p_1\cdot k-(v\cdot k)(v\cdot p_1)\right)}{\sqrt{2} f_\pi f_K \sqrt{m_{D_s}}(v\cdot p_1+\Delta)(v\cdot p_1+v\cdot p_2+\Delta)} \\
& + \frac{\alpha_1 (v\cdot k)}{\sqrt{2} f_\pi f_K \sqrt{m_{D_s}}}\left(1+\frac{f_\pi f_K m_{K^\star}^4}{g_{K^\star}^2} BW_{K^{+\star}}(p_1+p_2)\right) \\
& - \frac{\sqrt{m_D} f_D \lambda g_v m_{K^\star}^2 \left(p_1\cdot k-(v\cdot k)(v\cdot p_1)\right)}{g_{K^\star}\sqrt{m_{D_s}}(v\cdot p_1+v\cdot p_2+\Delta)} BW_{K^{+\star}}(p_1+p_2)
\end{aligned}
\tag{A73}
$$

$$
\begin{aligned}
c' = & -\frac{\sqrt{m_D} f_D g}{\sqrt{2m_{D_s}^3} f_\pi f_K (v\cdot p_1+\Delta)}\left[p_1\cdot k + g\frac{(p_2\cdot k)(v\cdot p_1)-(p_1\cdot k)(v\cdot p_2)}{v\cdot p_1+v\cdot p_2+\Delta}\right] \\
& + \frac{\alpha_1 (p_1\cdot k-p_2\cdot k)}{\sqrt{2m_{D_s}^3} f_\pi f_K}\left(1+\frac{f_\pi f_K m_{K^\star}^4}{g_{K^\star}^2} BW_{K^{+\star}}(p_1+p_2)\right) \\
& - \frac{\sqrt{m_D} f_D \lambda g_v m_{K^\star}^2 \left((p_2\cdot k)(v\cdot p_1)-(p_1\cdot k)(v\cdot p_2)\right)}{\sqrt{m_{D_s}^3} g_{K^\star}(v\cdot p_1+v\cdot p_2+\Delta)} BW_{K^{+\star}}(p_1+p_2)
\end{aligned}
\tag{A74}
$$

$$
\begin{aligned}
h' = & -\frac{\sqrt{m_D} f_D g}{2\sqrt{2m_{D_s}^3} f_\pi f_K (v\cdot p_1+\Delta)}\left(1+g\frac{v\cdot k}{v\cdot p_1+v\cdot p_2+\Delta}\right) \\
& - \frac{\alpha_1}{\sqrt{2m_{D_s}^3} f_\pi f_K}\left(1+\frac{f_\pi f_K m_{K^\star}^4}{g_{K^\star}^2} BW_{K^{+\star}}(p_1+p_2)\right) \\
& - \frac{\sqrt{m_D} f_D \lambda g_v m_{K^\star}^2 (v\cdot k)}{2\sqrt{m_{D_s}^3} g_{K^\star}(v\cdot p_1+v\cdot p_2+\Delta)} BW_{K^{+\star}}(p_1+p_2)
\end{aligned}
\tag{A75}
$$

$\underline{D^+ \to K^+ \overline{K}^0 \gamma}$

$$A_1^{(s,s)} = -i f_D \frac{v\cdot p_1+v\cdot k}{(v\cdot k)(p_1\cdot k)} \tag{A76}$$

$$A_{1+2}^{(d,d)} = -i f_D \frac{v\cdot p_2-v\cdot p_1-v\cdot k}{(v\cdot k)(p_1\cdot k)} \tag{A77}$$

$$A_3^{(s,s)} = -i\sqrt{\frac{m_{D_s}}{m_D}} f_{D_s} g \frac{p_1\cdot p_2-(v\cdot p_1)(v\cdot p_2)+(v\cdot k)(M-v\cdot p_2)}{(v\cdot p_2+\Delta)(v\cdot k)(p_1\cdot k)} \tag{A78}$$

$$A_4^{(s,s)} = -i\frac{\sqrt{m_{D_s}} f_{D_s} g (v\cdot k)}{\sqrt{m_D}(v\cdot k+v\cdot p_2+\Delta)}\left[\frac{2\lambda'+\frac{1}{\sqrt{2}} g_v \lambda\left(\frac{g_\omega}{3m_\omega^2}-\frac{g_\rho}{m_\rho^2}\right)}{v\cdot k+\Delta} - \frac{2\lambda'-\frac{\sqrt{2}}{3} g_v \lambda \frac{g_\Phi}{m_\Phi^2}}{v\cdot p_2+\Delta}\right] \tag{A79}$$

$$A_6^{(d,d)} = -i2 f_D \frac{p_1\cdot p_2}{m_D (v\cdot k)} BW_{\rho^+}(p_1+p_2) \tag{A80}$$

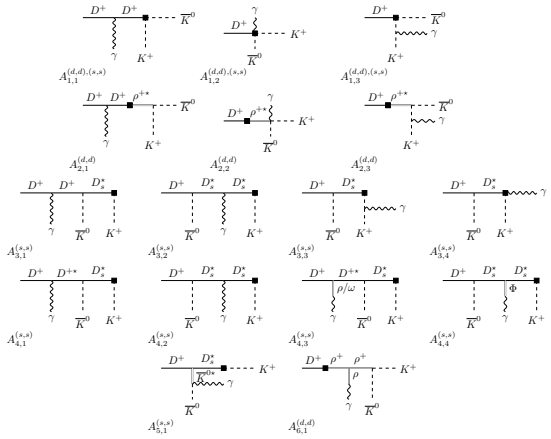

a) Contributions to the parity-even form factors A and E. Note that the diagrams A_1 have two different factorizations. Additionally, for each of the diagrams $A_{1,2}$, $A_{1,3}$, $A_{2,3}$, $A_{3,3}$ and $A_{3,4}$ there is another one where the photon is coupled via a vector meson.

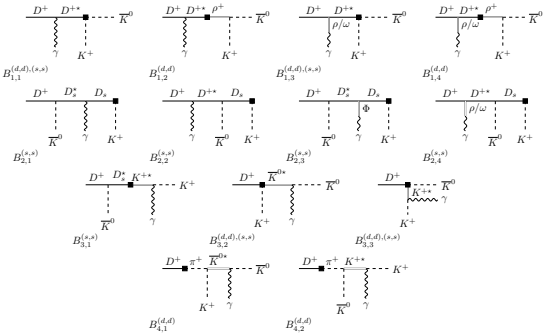

b) Contributions to the parity-odd form factors B and D. Note that the diagrams $B_{1,1/3}$ and $B_{3,2/3}$ have two different factorizations.

Figure 17: Feynman diagrams contributing to the decay $D^+ \to K^+\overline{K}^0\gamma$ within the SM.

$$B_1^{(s,s)} = \frac{f_D}{(v\cdot k+\Delta)}\left[2\lambda' + \frac{1}{\sqrt{2}} g_v \lambda \left(\frac{g_\omega}{3m_\omega^2} - \frac{g_\rho}{m_\rho^2}\right)\right]$$
$$B_1^{(d,d)} = -\frac{f_D}{v\cdot k+\Delta}\left[1 - m_\rho^2 BW_{\rho^+}(p_1+p_2)\right]\left[2\lambda' + \frac{1}{\sqrt{2}} g_v \lambda \left(\frac{g_\omega}{3m_\omega^2} - \frac{g_\rho}{m_\rho^2}\right)\right] \tag{A81}$$

$$B_2^{(s,s)} = \frac{\sqrt{m_{D_s}} f_{D_s} g(v\cdot p_1)}{\sqrt{m_D}(v\cdot k + v\cdot p_2)}\left[\frac{2\lambda' - \frac{\sqrt{2}}{3} g_v \lambda \frac{g_\Phi}{m_\Phi^2}}{v\cdot p_2+\Delta} + \frac{2\lambda' + \frac{1}{\sqrt{2}} g_v \lambda \left(\frac{g_\omega}{3m_\omega^2} - \frac{g_\rho}{m_\rho^2}\right)}{v\cdot k+\Delta}\right] \tag{A82}$$

$$B_3^{(s,s)} = -\frac{g_{K^\star} g_{K^{\pm\star}K^\pm\gamma}}{f_K}\left(f_D + g f_{D_s}\sqrt{\frac{m_{D_s}}{m_D}}\frac{m_D - v\cdot p_2}{v\cdot p_2+\Delta}\right) BW_{K^{+\star}}(p_1+k)$$
$$+ \frac{2 f_K (m_D \alpha_1 - \alpha_2 v\cdot p_1)}{\sqrt{m_D}} \frac{m_{K^\star}^2}{g_{K^\star}} g_{K^\star K\gamma} BW_{K^\star}(p_2+k)) \tag{A83}$$

$$B_3^{(d,d)} = \frac{f_D g_{K^\star}}{f_K}\left(g_{K^\star K\gamma} BW_{K^\star}(p_2+k) + g_{K^{\pm\star}K^\pm\gamma} BW_{K^{+\star}}(p_1+k)\right)$$

$$B_4^{(d,d)} = -\frac{m_D^2 f_D f_\pi}{(m_D^2 - m_\pi^2)} \frac{m_{K^\star}^2}{g_{K^\star}}\left(g_{K^\star K\gamma} BW_{K^\star}(p_2+k) + g_{K^{\pm\star}K^\pm\gamma} BW_{K^{+\star}}(p_1+k)\right) \tag{A84}$$

$$
\begin{aligned}
a' = & -\frac{f_D g^2\,(p_2\cdot k-(v\cdot k)(v\cdot p_2))}{f_K^2(v\cdot p_1+v\cdot p_2+\Delta)(v\cdot p_2+\Delta)}\\
& +\frac{\alpha_1(v\cdot k)}{f_K^2\sqrt{m_D}}\left(1+\frac{f_K^2 m_\rho^4}{g_\rho^2}BW_{\rho^+}(p_1+p_2)\right)\\
& -\frac{\sqrt{2}f_D\lambda g_v m_\rho^2\,(p_2\cdot k-(v\cdot k)(v\cdot p_2))}{g_\rho(v\cdot p_1+v\cdot p_2+\Delta)}BW_{\rho^+}(p_1+p_2)
\end{aligned}
\tag{A85}
$$

$$
\begin{aligned}
b' = & \frac{g}{f_K^2(v\cdot p_2+\Delta)}\left[\sqrt{\frac{m_{D_s}}{m_D}}f_{D_s}(v\cdot k)+f_D g\frac{p_1\cdot k-(v\cdot k)(v\cdot p_1)}{v\cdot p_1+v\cdot p_2+\Delta}\right]\\
& -\frac{\alpha_1(v\cdot k)}{f_K^2\sqrt{m_D}}\left(1+\frac{f_K^2 m_\rho^4}{g_\rho^2}BW_{\rho^+}(p_1+p_2)\right)\\
& +\frac{\sqrt{2}f_D\lambda g_v m_\rho^2\,(p_1\cdot k-(v\cdot k)(v\cdot p_1))}{g_\rho(v\cdot p_1+v\cdot p_2+\Delta)}BW_{\rho^+}(p_1+p_2)
\end{aligned}
\tag{A86}
$$

$$
\begin{aligned}
c' = & -\frac{g}{f_K^2 m_D(v\cdot p_2+\Delta)}\left[\sqrt{\frac{m_{D_s}}{m_D}}f_{D_s}(p_2\cdot k)-f_D g\frac{(p_2\cdot k)(v\cdot p_1)-(p_1\cdot k)(v\cdot p_2)}{v\cdot p_1+v\cdot p_2+\Delta}\right]\\
& -\frac{\alpha_1(p_1\cdot k-p_2\cdot k)}{\sqrt{m_D^3}f_K^2}\left(1+\frac{f_K^2 m_\rho^4}{g_\rho^2}BW_{\rho^+}(p_1+p_2)\right)\\
& +\frac{\sqrt{2}f_D\lambda g_v m_\rho^2\,((p_2\cdot k)(v\cdot p_1)-(p_1\cdot k)(v\cdot p_2))}{g_\rho m_D(v\cdot p_1+v\cdot p_2+\Delta)}BW_{\rho^+}(p_1+p_2)
\end{aligned}
\tag{A87}
$$

$$
\begin{aligned}
h' = & \frac{g}{2f_K^2 m_D(v\cdot p_2+\Delta)}\left(\sqrt{\frac{m_{D_s}}{m_D}}f_{D_s}+f_D g\frac{v\cdot k}{v\cdot p_1+v\cdot p_2+\Delta}\right)\\
& +\frac{\alpha_1}{\sqrt{m_D^3}f_K^2}\left(1+\frac{f_K^2 m_\rho^4}{g_\rho^2}BW_{\rho^+}(p_1+p_2)\right)\\
& +\frac{f_D\lambda g_v m_\rho^2\,(v\cdot k)}{\sqrt{2}g_\rho m_D(v\cdot p_1+v\cdot p_2+\Delta)}BW_{\rho^+}(p_1+p_2)
\end{aligned}
\tag{A88}
$$

3. Doubly Cabibbo-suppressed decay modes

$\underline{D^+\to\pi^+K^0\gamma}$

$$
\begin{aligned}
A_{1+2}^{(d,s)} &= -if_D\frac{v\cdot p_2-v\cdot p_1-v\cdot k}{(v\cdot k)(p_1\cdot k)}\\
A_6^{(d,s)} &= -i2f_D\frac{p_1\cdot p_2}{m_D(v\cdot k)}BW_{K^{\star+}}(p_1+p_2)
\end{aligned}
\tag{A89}
$$

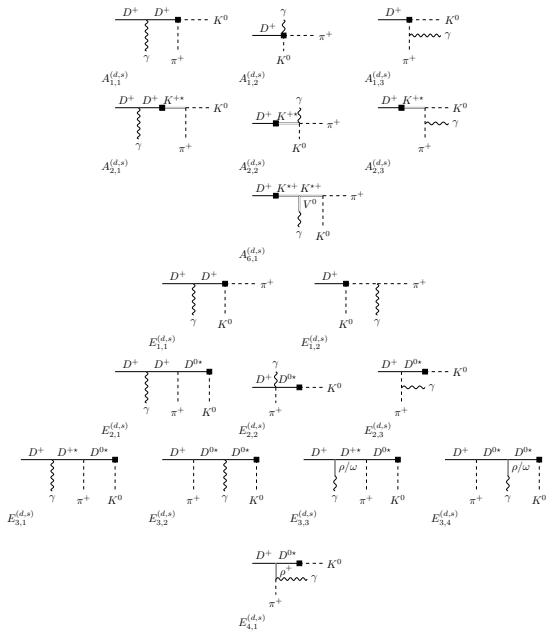

a) Contributions to the parity-even form factors A and E. Additionally, for each of the diagrams $A_{1,2}$, $A_{1,3}$, $A_{2,3}$, $E_{1,2}$ und $E_{2,3}$ there is another one where the photon is coupled via a vector meson.

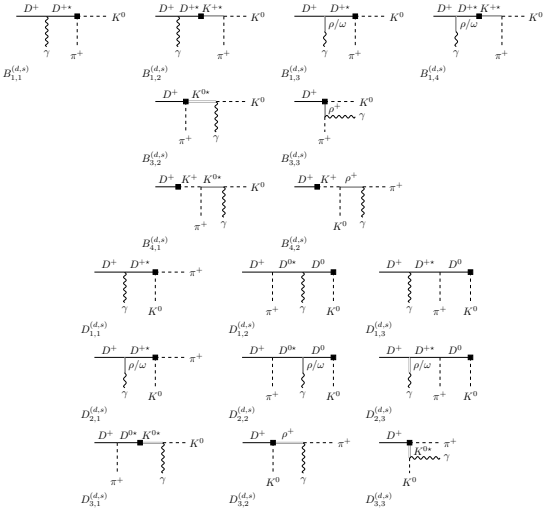

b) Contributions to the parity-odd form factors B and D.

Figure 18: Feynman diagrams contributing to the decay $D^+ \to \pi^+ K^0 \gamma$ within the SM.

$$E_1^{(d,s)} = -i\frac{f_D f_K}{f_\pi}\frac{v\cdot p_2}{(v\cdot k)(p_1\cdot k)} \tag{A90}$$

$$E_2^{(d,s)} = -i\frac{f_D f_K g}{f_\pi}\frac{p_1\cdot p_2 - (v\cdot p_1)(v\cdot p_2) + (v\cdot k)(m_D - v\cdot p_2)}{(v\cdot k + v\cdot p_1 + \Delta)(v\cdot k)(p_1\cdot k)} \tag{A91}$$

$$E_3^{(d,s)} = -i\frac{f_D f_K g (v\cdot k)}{f_\pi (v\cdot k + v\cdot p_1 + \Delta)}\left[\frac{2\lambda' + \frac{1}{\sqrt{2}} g_v \lambda \left(\frac{g_\omega}{3m_\omega^2} + \frac{g_\rho}{m_\rho^2}\right)}{v\cdot p_1 + \Delta} - \frac{2\lambda' + \frac{1}{\sqrt{2}} g_v \lambda \left(\frac{g_\omega}{3m_\omega^2} - \frac{g_\rho}{m_\rho^2}\right)}{v\cdot k + \Delta}\right] \tag{A92}$$

$$B_1^{(d,s)} = -\frac{f_D}{v\cdot k + \Delta}\left[1 - m_{K^\star}^2 BW_{K^{+\star}}(p_1+p_2)\right]\left[2\lambda' + \frac{g_v\lambda}{\sqrt{2}}\left(\frac{g_\omega}{3m_\omega^2} - \frac{g_\rho}{m_\rho^2}\right)\right] \tag{A93}$$

$$B_3^{(d,s)} = \frac{f_D g_{K^\star}}{f_\pi} g_{K^\star K\gamma} BW_{K^\star}(p_2+k) + \frac{f_D g_\rho}{f_K} g_{\rho^\pm\pi^\pm\gamma} BW_{\rho^+}(p_1+k) \tag{A94}$$

$$B_4^{(d,s)} = -\frac{m_D^2 f_D f_K}{(m_D^2 - m_K^2)}\left(\frac{m_{K^\star}^2}{g_{K^\star}} g_{K^\star K\gamma} BW_{K^\star}(p_2+k) + \frac{m_\rho^2}{g_\rho} g_{\rho^\pm\pi^\pm\gamma} BW_{\rho^+}(p_1+k)\right) \tag{A95}$$

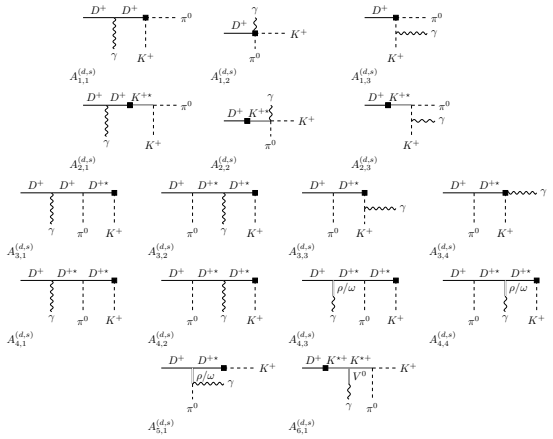

a) Contributions to the parity-even form factors A and E. Note that the diagrams A_1 have two different factorizations. Additionally, for each of the diagrams $A_{1,2}$, $A_{1,3}$, $A_{2,3}$, $A_{3,3}$ and $A_{3,4}$ there is another one where the photon is coupled via a vector meson.

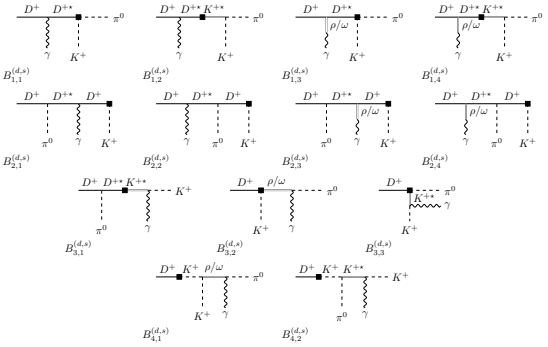

b) Contributions to the parity-odd form factors B and D. Note that the diagrams $B_{1,1/3}$ and $B_{3,2/3}$ have two different factorizations.

Figure 19: Feynman diagrams contributing to the decay $D^+ \to K^+\pi^0\gamma$ within the SM.

$$D_1^{(d,s)} = -2\frac{f_D f_K}{f_\pi}\lambda' \left[\frac{1}{v\cdot k+\Delta} + \frac{g(v\cdot p_2)}{v\cdot k + v\cdot p_1}\left(\frac{1}{v\cdot k+\Delta}+\frac{1}{v\cdot p_1+\Delta}\right)\right] \tag{A96}$$

$$D_2^{(d,s)} = -\frac{f_D f_K g_v \lambda}{\sqrt{2} f_\pi}\left[\frac{\frac{g_\omega}{3m_\omega^2}-\frac{g_\rho}{m_\rho^2}}{v\cdot k+\Delta} + \frac{g(v\cdot p_2)}{v\cdot k + v\cdot p_1}\left(\frac{\frac{g_\omega}{3m_\omega^2}-\frac{g_\rho}{m_\rho^2}}{v\cdot k+\Delta}+\frac{\frac{g_\omega}{3m_\omega^2}+\frac{g_\rho}{m_\rho^2}}{v\cdot p_1+\Delta}\right)\right] \tag{A97}$$

$$\begin{aligned} D_3^{(d,s)} = {} & \frac{f_D g_{K^\star} g_{K^\star K\gamma}}{f_\pi}\left(1+g\frac{m_D - v\cdot p_1}{v\cdot p_1+\Delta}\right) BW_{K^\star}(p_2+k) \\ & - \frac{2 f_K\left(m_D\alpha_1 - \alpha_2 v\cdot p_2\right)}{\sqrt{m_D}}\frac{m_\rho^2}{g_\rho} g_{\rho^\pm\pi^\pm\gamma} BW_{\rho^+}(p_1+k) \end{aligned} \tag{A98}$$

$\underline{D^+ \to K^+\pi^0\gamma}$

$$A_{1+2}^{(d,s)} = i\frac{f_D}{\sqrt{2}}\frac{v\cdot p_2 - v\cdot p_1 - v\cdot k}{(v\cdot k)(p_1\cdot k)} + i\frac{f_D f_K}{\sqrt{2} f_\pi}\frac{v\cdot p_1 + v\cdot k}{(v\cdot k)(p_1\cdot k)} \tag{A99}$$

$$A_3^{(d,s)} = i\frac{f_D f_K g}{\sqrt{2} f_\pi}\frac{p_1\cdot p_2 - (v\cdot p_1)(v\cdot p_2) + (v\cdot k)(M - v\cdot p_2)}{(v\cdot p_2+\Delta)(v\cdot k)(p_1\cdot k)} \tag{A100}$$

$$A_4^{(d,s)} = i\frac{f_D f_K g(v\cdot k)}{f_\pi(v\cdot k + v\cdot p_2+\Delta)}\left[\frac{\sqrt{2}\lambda' + \frac{1}{2}g_v\lambda\left(\frac{g_\omega}{3m_\omega^2}-\frac{g_\rho}{m_\rho^2}\right)}{v\cdot k+\Delta} - \frac{\sqrt{2}\lambda' + \frac{1}{2}g_v\lambda\left(\frac{g_\omega}{3m_\omega^2}-\frac{g_\rho}{m_\rho^2}\right)}{v\cdot p_2+\Delta}\right] \tag{A101}$$

$$A_6^{(d,s)} = i\sqrt{2} f_D \frac{p_1\cdot p_2}{m_D(v\cdot k)} BW_{K^{\star+}}(p_1+p_2) \tag{A102}$$

$$B_1^{(d,s)} = \frac{f_D}{v\cdot k+\Delta}\left[1-\frac{f_K}{f_\pi}-m_{K^\star}^2 BW_{K^{+\star}}(p_1+p_2)\right]\left[\sqrt{2}\lambda'+\frac{1}{2}g_v\lambda\left(\frac{g_\omega}{3m_\omega^2}-\frac{g_\rho}{m_\rho^2}\right)\right] \tag{A103}$$

$$B_2^{(d,s)} = -\frac{f_D f_K g(v\cdot p_1)}{f_\pi(v\cdot k+v\cdot p_2)}\left[\frac{\sqrt{2}\lambda'+\frac{1}{2}g_v\lambda\left(\frac{g_\omega}{3m_\omega^2}-\frac{g_\rho}{m_\rho^2}\right)}{v\cdot p_2+\Delta}+\frac{\sqrt{2}\lambda'+\frac{1}{2}g_v\lambda\left(\frac{g_\omega}{3m_\omega^2}-\frac{g_\rho}{m_\rho^2}\right)}{v\cdot k+\Delta}\right] \tag{A104}$$

$$\begin{aligned}B_3^{(d,s)} &= \frac{f_D g_{K^\star} g_{K^{\pm\star}K^\pm\gamma} g(m_D-v\cdot p_2)}{\sqrt{2}f_\pi(v\cdot p_2+\Delta)}BW_{K^{+\star}}(p_1+k)\\ &+\frac{\sqrt{2}f_K(m_D\alpha_1-\alpha_2 v\cdot p_1)}{\sqrt{m_D}}\left(\frac{m_\omega^2}{g_\omega}g_{\omega\pi\gamma}BW_\omega(p_2+k)-\frac{m_\rho^2}{g_\rho}g_{\rho\pi\gamma}BW_\rho(p_2+k)\right)\\ &-\frac{f_D}{\sqrt{2}}\left(\frac{g_\rho}{f_K}g_{\rho\pi\gamma}BW_\rho(p_2+k)+\frac{g_\omega}{f_K}g_{\omega\pi\gamma}BW_\omega(p_2+k)\right)\end{aligned} \tag{A105}$$

$$B_4^{(d,s)} = \frac{m_D^2 f_D f_K}{\sqrt{2}(m_D^2-m_K^2)}\left(\frac{m_\rho^2}{g_\rho}g_{\rho\pi\gamma}BW_\rho(p_2+k)+\frac{m_\omega^2}{g_\omega}g_{\omega\pi\gamma}BW_\omega(p_2+k)+\frac{2m_{K^\star}^2}{g_{K^\star}}g_{K^{\pm\star}K^\pm\gamma}BW_{K^{+\star}}(p_1+k)\right) \tag{A106}$$

$\underline{D_s \to K^+K^0\gamma}$

$$A_1^{(d,s)} = -if_{D_s}\frac{v\cdot p_1+v\cdot k}{(v\cdot k)(p_1\cdot k)} \tag{A107}$$

$$A_3^{(d,s)} = -i\sqrt{\frac{m_D}{m_{D_s}}}f_D g\frac{p_1\cdot p_2-(v\cdot p_1)(v\cdot p_2)+(v\cdot k)(m_D-v\cdot p_2)}{(v\cdot p_2+\Delta)(v\cdot k)(p_1\cdot k)} \tag{A108}$$

$$A_4^{(d,s)} = -i\sqrt{\frac{m_D}{m_{D_s}}}\frac{f_D g(v\cdot k)}{v\cdot k+v\cdot p_2+\Delta}\left[\frac{2\lambda'-\frac{\sqrt{2}}{3}g_v\lambda\frac{g_\Phi}{m_\Phi^2}}{v\cdot k+\Delta}-\frac{2\lambda'+\frac{1}{\sqrt{2}}g_v\lambda\left(\frac{g_\omega}{3m_\omega^2}-\frac{g_\rho}{m_\rho^2}\right)}{v\cdot p_2+\Delta}\right] \tag{A109}$$

$$E_1^{(d,s)} = -if_{D_s}\frac{v\cdot p_2}{(v\cdot k)(p_1\cdot k)} \tag{A110}$$

$$E_2^{(d,s)} = -i\sqrt{\frac{m_D}{m_{D_s}}}f_D g\frac{p_1\cdot p_2-(v\cdot p_1)(v\cdot p_2)+(v\cdot k)(m_D-v\cdot p_2)}{(v\cdot k+v\cdot p_1+\Delta)(v\cdot k)(p_1\cdot k)} \tag{A111}$$

$$E_3^{(d,s)} = -i\sqrt{\frac{m_D}{m_{D_s}}}\frac{f_D g(v\cdot k)}{v\cdot k+v\cdot p_1+\Delta}\left[\frac{2\lambda'+\frac{1}{\sqrt{2}}g_v\lambda\left(\frac{g_\omega}{3m_\omega^2}+\frac{g_\rho}{m_\rho^2}\right)}{v\cdot p_1+\Delta}-\frac{2\lambda'-\frac{\sqrt{2}}{3}g_v\lambda\frac{g_\Phi}{m_\Phi^2}}{v\cdot k+\Delta}\right] \tag{A112}$$

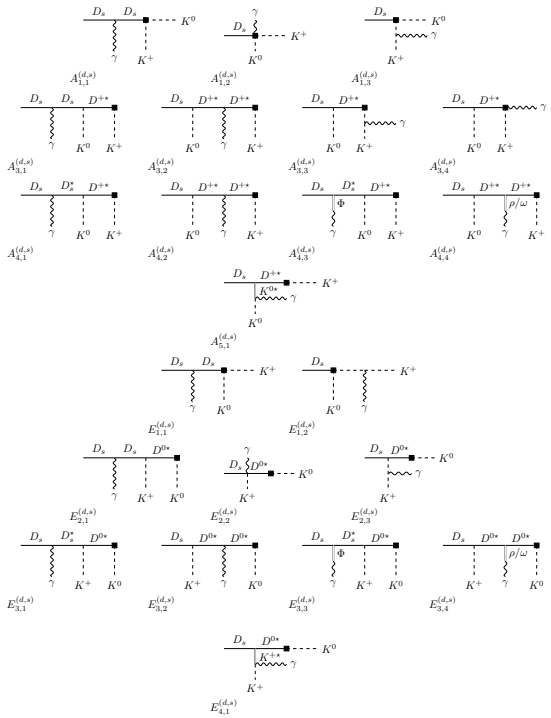

a) Contributions to the parity-even form factors A and E. For each of the diagrams $A_{1,2}$, $A_{1,3}$, $A_{3,3}$, $A_{3,4}$, $E_{1,2}$ und $E_{2,3}$ there is another one where the photon is coupled via a vector meson.

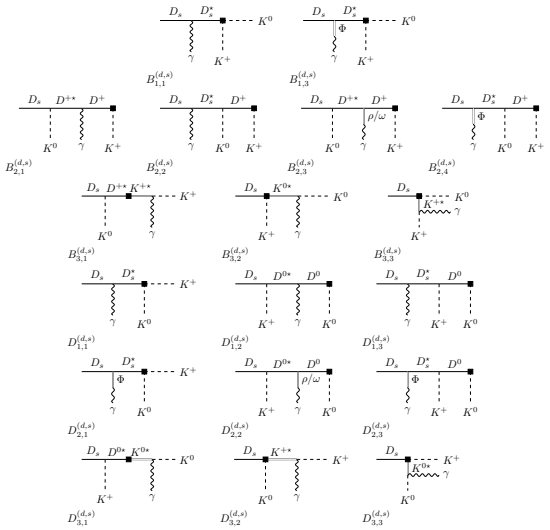

b) Contributions to the parity-odd form factors B and D.

Figure 20: Feynman diagrams contributing to the decay $D_s \to K^+K^0\gamma$ within the SM.

$$B_1^{(d,s)} = \frac{f_{D_s}}{v\cdot k+\Delta}\left[2\lambda' - \frac{\sqrt{2}}{3}g_v\lambda\frac{g_\Phi}{m_\Phi^2}\right] \tag{A113}$$

$$B_2^{(d,s)} = \sqrt{\frac{m_D}{m_{D_s}}}\frac{f_D g(v\cdot p_1)}{v\cdot k + v\cdot p_2}\left[\frac{2\lambda' + \frac{1}{\sqrt{2}}g_v\lambda\left(\frac{g_\omega}{3m_\omega^2} - \frac{g_\rho}{m_\rho^2}\right)}{v\cdot p_2+\Delta} + \frac{2\lambda' - \frac{\sqrt{2}}{3}g_v\lambda\frac{g_\Phi}{m_\Phi^2}}{v\cdot k+\Delta}\right] \tag{A114}$$

$$\begin{aligned} B_3^{(d,s)} = &-\frac{g_{K^\star}g_{K^{\pm\star}K^\pm\gamma}}{f_K}\left(f_{D_s} + \sqrt{\frac{m_D}{m_{D_s}}}f_D g\frac{m_{D_s}-v\cdot p_2}{v\cdot p_2+\Delta}\right)BW_{K^{+\star}}(p_1+k) \\ &+ \frac{2f_K(m_{D_s}\alpha_1 - \alpha_2 v\cdot p_1)}{\sqrt{m_{D_s}}}\frac{m_{K^\star}^2}{g_{K^\star}}g_{K^\star K\gamma}BW_{K^\star}(p_2+k) \end{aligned} \tag{A115}$$

$$D_1^{(d,s)} = -2\lambda' \left[\frac{f_{D_s}}{v\cdot k+\Delta} + \sqrt{\frac{m_D}{m_{D_s}}} \frac{f_D g(v\cdot p_2)}{v\cdot k + v\cdot p_1} \left(\frac{1}{v\cdot k+\Delta} + \frac{1}{v\cdot p_1+\Delta} \right) \right] \tag{A116}$$

$$D_2^{(d,s)} = -g_v\lambda \left[\frac{-f_{D_s}\frac{\sqrt{2}}{3}\frac{g_\Phi}{m_\Phi^2}}{v\cdot k+\Delta} + \sqrt{\frac{m_D}{m_{D_s}}} \frac{f_D g(v\cdot p_2)}{v\cdot k + v\cdot p_1} \left(\frac{-\frac{\sqrt{2}}{3}\frac{g_\Phi}{m_\Phi^2}}{v\cdot k+\Delta} + \frac{\frac{1}{\sqrt{2}}\left(\frac{g_\omega}{3m_\omega^2}+\frac{g_\rho}{m_\rho^2}\right)}{v\cdot p_1+\Delta} \right) \right] \tag{A117}$$

$$\begin{aligned} D_3^{(d,s)} = {} & \frac{g_{K^\star}g_{K^\star K\gamma}}{f_K} \left(f_{D_s} + \sqrt{\frac{m_D}{m_{D_s}}} f_D g \frac{m_{D_s} - v\cdot p_1}{v\cdot p_1+\Delta} \right) BW_{K^\star}(p_2+k) \\ & - \frac{2f_K\left(m_{D_s}\alpha_1 - \alpha_2 v\cdot p_2\right)}{\sqrt{m_{D_s}}} \frac{m_{K^\star}^2}{g_{K^\star}} g_{K^{\pm\star}K^\pm\gamma} BW_{K^{\pm\star}}(p_1+k) \end{aligned} \tag{A118}$$

Appendix B: Differences with respect to [11]

We provide a list of some differences between our form factors and those obtained in Ref. [11]. More comments are given in [10].

1. The contributions of the diagrams $A_{4,1}^+$ and $C_{4,1}^+$ vanish in our calculation.

2. Missing global minus sign in C_2^+.

3. We believe that there are diagrams that have not been shown in Ref. [11]: For each of the diagrams $A_{1,2}^+$, $A_{1,3}^+$, $A_{3,3}^+$, $A_{3,4}^+$, $E_{1,2}^0$ and $E_{2,3}^0$ there is another one in which the photon couples via a vector meson. However, we obtain the same form factors for the bremsstrahlung contributions.

4. We obtain a relative minus sign for each vector meson in a diagram; however, we get the same relative signs for $R_\gamma^{0/+}$ as given in Eqs. (24) and (25) [28].

---

[1] G. Burdman, E. Golowich, J. L. Hewett and S. Pakvasa, Phys. Rev. D **66**, 014009 (2002) doi:10.1103/PhysRevD.66.014009 [arXiv:hep-ph/0112235 [hep-ph]].

[2] A. Cerri *et al*, CERN Yellow Rep. Monogr. **7**, 867-1158 (2019) doi:10.23731/CYRM-2019-007.867 [arXiv:1812.07638 [hep-ph]].

[3] E. Kou *et al.* [Belle-II Collaboration], PTEP **2019**, no. 12, 123C01 (2019) [arXiv:1808.10567 [hep-ex]].

[4] M. Ablikim *et al.*, Chin. Phys. C **44** (2020) no.4, 040001 [arXiv:1912.05983 [hep-ex]].

[5] S. Fajfer and N. Košnik, Eur. Phys. J. C **75**, no.12, 567 (2015) doi:10.1140/epjc/s10052-015-3801-2 [arXiv:1510.00965 [hep-ph]].

[6] S. De Boer and G. Hiller, Phys. Rev. D **98** (2018) no.3, 035041 doi:10.1103/PhysRevD.98.035041 [arXiv:1805.08516 [hep-ph]].

[7] R. Bause, M. Golz, G. Hiller and A. Tayduganov, Eur. Phys. J. C **80**, no.1, 65 (2020) [erratum: Eur. Phys. J. C **81**, no.3, 219 (2021)] doi:10.1140/epjc/s10052-020-7621-7 [arXiv:1909.11108 [hep-ph]].

[8] S. de Boer and G. Hiller, Eur. Phys. J. C **78**, no.3, 188 (2018) doi:10.1140/epjc/s10052-018-5682-7 [arXiv:1802.02769 [hep-ph]].

[9] N. Adolph, G. Hiller and A. Tayduganov, Phys. Rev. D **99**, no. 7, 075023 (2019) doi:10.1103/PhysRevD.99.075023 [arXiv:1812.04679 [hep-ph]].

[10] N. Adolph, J. Brod and G. Hiller, Eur. Phys. J. C **81** (2021) no.1, 45 doi:10.1140/epjc/s10052-021-08832-3 [arXiv:2009.14212 [hep-ph]].

[11] S. Fajfer, A. Prapotnik and P. Singer, Phys. Rev. D **66** (2002) 074002 doi:10.1103/PhysRevD.66.074002 [hep-ph/0204306].

[12] S. Fajfer, A. Prapotnik and P. Singer, Phys. Lett. B **550** (2002) 77 doi:10.1016/S0370-2693(02)02964-7 [hep-ph/0210423].

[13] S. de Boer and G. Hiller, JHEP **1708** (2017) 091 doi:10.1007/JHEP08(2017)091 [arXiv:1701.06392 [hep-ph]].

[14] M. Beneke, G. Buchalla, M. Neubert and C. T. Sachrajda, Nucl. Phys. B **591** (2000), 313-418 doi:10.1016/S0550-3213(00)00559-9 [arXiv:hep-ph/0006124 [hep-ph]].

[15] S. W. Bosch and G. Buchalla, Nucl. Phys. B **621** (2002) 459 doi:10.1016/S0550-3213(01)00580-6 [hep-ph/0106081].

[16] S. Descotes-Genon and C. T. Sachrajda, Nucl. Phys. B **650** (2003) 356 doi:10.1016/S0550-3213(02)01066-0 [hep-ph/0209216].

[17] C. Bruch, A. Khodjamirian and J. H. Kuhn, Eur. Phys. J. C **39** (2005) 41 doi:10.1140/epjc/s2004-02064-3 [hep-ph/0409080].

[18] D. R. Boito, R. Escribano and M. Jamin, Eur. Phys. J. C **59** (2009) 821 doi:10.1140/epjc/s10052-008-0834-9 [arXiv:0807.4883 [hep-ph]].

[19] F. E. Low, Phys. Rev. **110** (1958) 974 doi:10.1103/PhysRev.110.974

[20] V. Del Duca Nucl. Phys. B **345** (1990) 369 doi:10.1016/0550-3213(90)90392-Q

[21] M. Tanabashi *et al.* [Particle Data Group], Phys. Rev. D **98** (2018) no.3, 030001. doi:10.1103/PhysRevD.98.030001

[22] M. B. Wise, Phys. Rev. D **45**, (1992) R2188 doi:10.1103/PhysRevD.45.R2188

[23] G. Burdman, J. F. Donoghue Nucl. Phys. B **280** (1992) 287 doi:10.1016/0370-2693(92)90068-F

[24] T. M. Yan *et al.* Phys. Rev. D **46**, (1992) 1148 doi:10.1103/PhysRevD.46.1148

[25] R. Casalbuoni et al., Phys. Lett. B **299**, 139 (1993) doi:10.1016/0370-2693(93)90895-O; Phys. Rep. **281**, 145 (1997) doi:10.1016/S0370-1573(96)00027-0

[26] E. Golowich and S. Pakvasa, Phys. Rev. D **51** (1995), 1215-1223 doi:10.1103/PhysRevD.51.1215 [arXiv:hep-ph/9408370 [hep-ph]].

[27] A. Abdesselam *et al.* [Belle Collaboration], Phys. Rev. Lett. **118** (2017) no.5, 051801 doi:10.1103/PhysRevLett.118.051801 [arXiv:1603.03257 [hep-ex]].

[28] B. Bajc, S. Fajfer and R. J. Oakes, Phys. Rev. D **51** (1995) 2230 doi:10.1103/PhysRevD.51.2230 [hep-ph/9407388].